HHS Public Access

Author manuscript

J Comp Neurol. Author manuscript; available in PMC 2020 November 01.

Published in final edited form as:

J Comp Neurol. 2019 November 01; 527(16): 2761–2789. doi:10.1002/cne.24706.

Terminal Organization of the Corticospinal Projection from the Lateral Premotor Cortex to the Cervical Enlargement (C5-T1) in Rhesus Monkey

R.J. Morecraft[1], **J. Ge**[1], **K.S. Stilwell-Morecraft**[1], **DL Rotella**[2], **M.A. Pizzimenti**[2,3], **W.G. Darling**[2]

[1]Division of Basic Biomedical Sciences, Laboratory of Neurological Sciences, The University of South Dakota, Sanford School of Medicine, Vermillion, South Dakota 57069.

[2]Department of Health and Human Physiology, Motor Control Laboratories, The University of Iowa, Iowa City, Iowa 52242.

[3]Department of Anatomy and Cell Biology, Carver College of Medicine, The University of Iowa, Iowa City, Iowa 52242.

Abstract

High resolution tract tracing and stereology were used to study the terminal organization of the corticospinal projection (CSP) from the ventral (v) and dorsal (d) regions of the lateral premotor cortex (LPMC) to spinal levels C5-T1. The LPMCv CSP originated from the post-arcuate sulcus region, was bilateral, sparse, and primarily targeted the dorsolateral and ventromedial sectors of contralateral lamina VII. The convexity/lateral part of LPMCv did not project below C2. Thus, very little LPMCv corticospinal output reaches the cervical enlargement. In contrast, the LPMCd CSP was 5X more prominent in terminal density. Bilateral terminal labeling occurred in the medial sectors of lamina VII and adjacent lamina VIII, where propriospinal neurons with long-range bilateral axon projections reside. Notably, lamina VIII also harbors axial motoneurons. Contralateral labeling occurred in the lateral sectors of lamina VII and the dorsomedial quadrant of lamina IX, noted for harboring proximal upper limb flexor motoneurons. Segmentally, the CSP to contralateral laminae VII and IX preferentially innervated C5-C7, which supplies shoulder, elbow and wrist musculature. In contrast, terminations in axial-related lamina VIII were distributed bilaterally throughout all cervical enlargement levels, including C8 and T1. These findings demonstrate the LPMCd CSP is structured to influence axial and proximal upper limb movements, supporting Kuypers conceptual view of the LPMCd CSP being a major component of

ADDRESS CORRESPONDENCE: Dr. Robert J. Morecraft, Division of Basic Biomedical Sciences, Director, Laboratory of Neurological Sciences, The University of South Dakota, Sanford School of Medicine, Vermillion, SD 57069, USA. (Fax 605-677-6381; rmorecra@usd.edu).

Role of authors. All authors listed on the paper contributed significantly to the elaboration of the paper and/or to the research that led to preparation of the manuscript. All authors had full access to all the data in the study and take responsibility for the integrity of the data and the accuracy of the data analysis. Study concept and design: RJM and WGD. Development of data: RJM, JG, KSS-M. Acquisition of data: JG, RJM, KSS-M; Interpretation of data: RJM, WGD, JG, KSS-M, MAP, DLR. Drafting of the manuscript: RJM, WGD, JG, KSS-M, MAP, DLR. Study supervision: RJM.

Data Availability Statement: All data for this study have been included in the main document and its supporting materials.

Conflict of interest statement.

All authors do not have any conflict of interest that could inappropriately influence, or be perceived to influence, this work.

the medial motor control system. Thus, distal upper extremity control influenced by LPMC, including grasping and manipulation, must occur through indirect neural network connections such as corticocortical, subcortical, or intrinsic spinal circuits.

Graphical Abstract

Using high resolution tract tracing, the authors demonstrate the dorsal lateral premotor cortex (LPMCd) gives rise to a prominent bilateral corticospinal projection (CSP) involving the ventromedial (red) and lateral (blue) gray matter regions. In contrast a weaker bilateral CSP arose from the peri-arcuate region of ventral lateral premotor cortex (LPMCv).

Keywords

Pyramidal Tract; Frontal Lobe; Upper Extremity Movement; Reaching; RRID:AB_2336819; RRID:SCR_1775; RRID:SCR_002526; RRID:SCR_004314; Spinal Cord

INTRODUCTION

Armed with what is now considered rudimentary tract tracing methodology, Henricus Kuypers designed a series of experiments in the 1960's aimed to elucidate the anatomical organization of the monkey corticospinal projection (CSP) from the frontal lobe (Kuypers, 1960, 1962, 1964; Kuypers & Brinkman, 1970). He discovered two major patterns of degenerating corticospinal terminals following isolated resection of different parts of the frontal motor cortex involved with upper extremity motor control. The first pattern was predominately contralateral, characterized by a dorsolateral distribution of axon terminals ending in the dorsal and lateral parts of the intermediate zone (lamina VII) and the lateral motoneuronal cell group of the anterior horn (lamina IX). In contrast, the second pattern was bilateral, characterized by a ventromedial distribution of spinal terminations occupying the medial parts of the intermediate zone (lamina VII) and the medial motoneuronal cell group of the anterior horn (lamina VIII). Importantly, he also recognized that these diverse patterns of spinal terminations, when directly related to the anatomical arrangement of the spinal cord nuclei, could predict the functional influence of each frontal motor area corticospinal projection (Kuypers & Brinkman, 1970; Kuypers, 1982). These predictions correlated closely with the peripheral movement patterns elicited by electrophysiological stimulation of localized parts of the lateral frontal motor cortex (Kwan, MacKay, Murphy, & Wong, 1978b; Woolsey et al., 1952).

Specifically, the dorsolateral CSP pattern was observed to originate from the arm/hand representation of the primary motor cortex (M1) (Kuypers, 1960; Kuypers & Brinkman, 1970). At the spinal cord level, the terminal pattern included direct contralateral projections to spinal lamina IX, which at lower segmental levels of the cervical enlargement, harbor motoneurons innervating muscles acting on the wrist and fingers. This was complemented by a topographically specific contralateral CSP M1 to the dorsal and lateral parts of lamina VII, which harbor spinal propriospinal neurons with short-range ipsilateral axon projections which also innervate lamina IX motoneurons (Sterling & Kuypers, 1968). Physiological findings were in accordance with this arrangement as stimulation of the arm/hand area of

M1 elicited contralateral movements of the distal upper extremity including wrist and digit movements (Kwan et al., 1978b; Woolsey et al., 1952). Collectively, these observations led Kuypers to designate this CSP as being an integral part of a “lateral motor system” structured to steer movements of the contralateral distal upper extremity (Kuypers, 1982). We recently verified these M1 CSP findings using stereology and modern high resolution tract tracing techniques, but also documented several new structural characteristics of this CSP providing further support for the lateral motor system concept (Morecraft et al., 2013). Some important observations include: 1) The lamina IX projection gradually increased from C5 to C8/T1 whereas the projection to lamina VII gradually decreased within the same segmental span. 2) The spatial distribution of lamina IX terminals was topographically restricted to the dorsal quadrants at C5-C7 which contain proximal and distal flexor motor neurons. However this changed at C8 and T1 to a more dispersed pattern involving all quadrants, thus providing widespread innervation of flexor, extensor, adductor and abductor motoneurons of the wrist and digits. 3) Ninety eight percent of the M1 arm/hand terminal boutons resided in contralateral cervical enlargement, underscoring the contralateral emphasis of the lateral motor system proposal.

In contrast, the ventromedial pattern of the CSP originated from the shoulder representation of M1 and dorsal region of the lateral premotor cortex (LPMCd) (Kuypers & Brinkman, 1970; Kuypers, 1982). The ventromedial projection system was characterized by bilateral spinal terminations ending in lamina VIII, which harbors axial motor neurons. This was complimented by dense bilateral projections to the ventromedial part of lamina VII, which was known to contain propriospinal neurons with long-range bilateral axon projections which also innervate lamina VIII motoneurons (Sterling & Kuypers, 1968). Electrophysiological stimulation of LPMCd and the shoulder/trunk region of the M1 was shown to elicit proximal movements of the upper extremity and axial movements involving the neck, shoulder, and trunk (Kwan et al., 1978b; Woolsey et al., 1952). Together, these observations led Kuypers to categorize this CSP as being part of a “medial motor system” designed to steer movements of the axial and proximal upper extremity (Kuypers, 1982).

It is surprising that the terminal organization of the CSP from the M1 shoulder and LPMCd regions have not been the subject of contemporary investigations applying high-resolution tract tracing approaches. Some important questions remain regarding the fundamental organization of the medial motor system CSP. For example, after LPMCd ablation, Kuypers reported heavy labeling in all regions of contralateral lamina VII but only in the medial region in the ipsilateral CSP (Kuypers & Brinkman, 1970). He was aware of the difficulty in differentiating degenerating axons in passage from terminal boutons, particularly in the dorsolateral part of the contralateral gray matter which precluded an accurate assessment of terminal density in this location. In addition, the limited sensitivity this technique did not permit topographical insight into the LPMCd CSP to lamina IX. Finally, whether the ventromedial CSP predominately innervates proximal limb segments of the cervical enlargement (C5-C7) more so than distal limb segments of the enlargement (C8-T1) remains an important question.

To address these issues, we designed an experimental study in the rhesus monkey to provide the first contemporary investigation examining the terminal organization of the LPMCd CSP

to the cervical enlargement (C5-T1) using high resolution dextran tract tracers and stereology. To facilitate this investigation, as in our previous study on the M1 CSP (Morecraft et al., 2013), we subdivided Rexed's laminae into multiple subsectors, including lamina VII into 5 subsectors and lamina IX into 4 quadrants. This enabled us to revisit Kuypers medial motor system concept from a corticospinal perspective, to further test hypotheses based on his theory of axial/proximal limb motor control. For comparative purposes, we also investigated the CSP to C5-T1 from LPMCv as anterograde and retrograde studies show a CSP arising from the dorsal part of LPMCv (e.g., Borra, Belmalih, Gerbella, Rozzi, & Luppino, 2010; Catsman-Berrevoets & Kuypers, 1976; Dum & Strick, 1991; Galea & Darian-Smith, 1994; Martino & Strick, 1987).

MATERIALS AND METHODS

The terminal distribution of the corticospinal projection (CSP) arising from the lateral premotor cortex (LPMC) to spinal levels C5-T1 was studied in 5 rhesus monkeys (*Macaca mulatta*) and 9 injection sites (Fig. 1; Table 1). The CSP from the dorsolateral premotor cortex (LPMCd) was studied in all 5 cases. In 3 of these cases (SDM54, SDM57 and SDM61), a relatively large injection site was made in LPMCd so that a potentially robust CSP could be evaluated. In case SDM77 a small injection site was made involving the transition region between the caudal region of LPMCd and rostral M1 to determine laterality of the CSP in this location compared to the injection sites located directly within LPMC. In case SDM72, the rostral most region of LPMCd known to contain CSP neurons (Catsman-Berrevoets & Kuypers, 1976; Dum & Strick, 1991; Galea & Darian-Smith, 1994; He, Dum, & Strick, 1993) was injected with 2 tracers, with one placed immediately anterior to the other, to determine if the LPMCd CSP varied in strength at rostral versus caudal levels. We also examined a potential CSP from the dorsal part of the ventrolateral premotor cortex (LPMCv) in 3 cases (SDM57, SDM61 and SDM72) because studies injecting retrograde tracers in the upper cervical levels (C1-C4) of the monkey spinal cord have shown labeled cells in this general cortical region (e.g. Galea & Darian-Smith, 1994; He et al., 1993; Murray & Coulter, 1981; Nudo & Masterton, 1990; Toyoshima & Sakai, 1982).

All experimental protocols were approved by The University of South Dakota Institutional Animal Care and Use Committee. All experimental and surgical procedures were conducted at the University of South Dakota and followed United States Department of Agriculture, National Institutes of Health, and Society for Neuroscience guidelines for the ethical treatment of animals.

Neurosurgery, Intracortical Microsimulation and Tract Tracer Injection

Preoperatively, each monkey was immobilized with atropine (0.5mg/kg) then ketamine hydrochloride (10mg/kg). Each subject was intubated, placed on a mechanical ventilator and anesthetized with a mixture of 1.0-1.5% isoflurane and surgical grade air/oxygen. Once deeply anesthetized, each animal was placed in a neurosurgical head holder and mannitol was administered intravenously (1.0-1.5g/kg) to reduce overall cortical volume and enhance surgical accessibility of the brain. Under sterile conditions and isoflurane anesthesia, a skin flap was made over the cranium followed by an oval bone flap positioned over the precentral

cortical region (McNeal et al., 2010; Morecraft et al., 2013; Morecraft, McNeal, Stilwell-Morecraft, Dvanajscak, et al., 2007). In all cases the precentral region, extending from the central sulcus to the cortex forming the arcuate sulcus, was mapped using intracortical microstimulation (ICMS) as previously described (McNeal et al., 2010; Morecraft et al., 2013; Morecraft, McNeal, Stilwell-Morecraft, Dvanajscak, et al., 2007) (Fig. 1). Current intensity ranged between 7 and 90 μA. Threshold currents were determined, and evoked movements were discrete isolated twitches, confined to specific body parts. The specific movements were recorded when agreed upon by at least two observers. After ICMS mapping, the anterograde neural tract tracer lucifer yellow dextran (LYD), fluorescein dextran (FD), or biotinylated dextran amine (BDA) (Molecular Probes, Eugene, OR) was injected into LPMCd or LPMCv surrounded by well-defined upper extremity and cranial motor responses. Graded pressure injections with a Hamilton microsyringe were made approximately 1.5-2.5 mm below the pial surface with total volumes ranging from 0.8μL to 1.2 μL (Table 1). The Hamilton syringe was held in a specially designed microdrive attached to a stabilized electrode micromanipulator (model 1460 Kopf Instruments, Tujunga, CA) and all injection penetrations were made perpendicular to the cortical surface. Three injections were placed in a triangular pattern approximately 1.5 mm apart in cases SDM57-FD, SDM61-FD and SDM54-BDA. In case SDM72, the 3 injections of each tracer (LYD, BDA and FD) were made in a medial to lateral pattern approximately 1.0 mm apart, as were the 2 injections in case SDM77-BDA. Following the injection procedure, the surgical field was irrigated with 0.9% sterile saline then gently swabbed. The dura was repositioned, closed with sutures and the bone flap replaced and anchored. To conclude the surgery, the temporalis muscle was sutured in place and the skin was closed using standard surgical technique. The animal was carefully monitored after surgery and penicillin (procaine G) was used as pre- and post-operative prophylaxis antibiotic. Buprenorphine (0.01 mg/kg) was used as a post-operative analgesic.

Tissue Processing

Following a survival period of 32-33 days after tract tracer injection, each monkey was anesthetized with an IP overdose of pentobarbital (50 mg/kg or more) and perfused transcardially with 0.9% saline. Saline infusion was followed by 2 liters of 4% paraformaldehyde in 0.1M phosphate buffer at pH 7.4 (PB) to fix the tissue. The first liter of paraformaldehyde fixative was administered rapidly and the second liter via slow drip. Then infusion of one liter each of 10% followed by 30% sucrose in 0.1M PB for tissue cryoprotection concluded the perfusion. The entire central nervous system was removed, placed in 30% sucrose in 0.1M PB and stored for 2 to 5 days at 4° C. During removal of the spinal cord region, several millimeters of each dorsal and ventral spinal root were intentionally left on the cord. Prior to blocking the tissue for microtome sectioning, the cortex, brainstem and spinal cord were photographed with metric calibration. Ventral and dorsal roots of the spinal cord were extended so their positions relative to the long axis of the cord could be clearly recorded for determining the segmental level locations and intersegment boundaries during the data analysis and reconstruction process.

In all cases, the cerebral cortex was frozen sectioned in the coronal plane on a sliding microtome (American Optical 860, Buffalo, NY, USA) at a thickness of 50 μm in cycles of

10, forming 10 complete series of evenly spaced tissue sections respectively. Each spinal cord was blocked from the central nervous system, frozen with dry ice and cut transversely (90° to its long axis) on the sliding microtome at a thickness of 50 μm in cycles of 6 or 8, with each forming a complete series of evenly spaced tissue sections respectively. For both the cortical and spinal cord sections, one series of tissue sections was mounted on subbed slides, dried and eventually stained for Nissl substance using thionin and coverslipped with Permount to evaluate cytoarchitectonic organization (Morecraft et al., 2013; Morecraft, Geula, & Mesulam, 1992).

In all monkeys involved in this study, BDA was injected into a cortical region of interest as was LYD and FD. Thus, subsequent series of tissue sections through the cortex and spinal cord were then processed using single (BDA alone) and double label (BDA + LYD; BDA + FD) immunohistochemical procedures for localization of the neural tracers (Morecraft, McNeal, Stilwell-Morecraft, Dvanajscak, et al., 2007). To accomplish this, one series of tissue sections from the cortex and spinal cord was used to process BDA alone (single labeling procedure) using the Vectastain Elite avidin-biotin complex (ABC) labeling procedure (PK-6100, Vector Laboratories, Burlingame, CA, USA) (RRID:AB_2336819) (Figs. 2G-I, 3A-C, G-I). Briefly, the tissue sections were rinsed in 0.05M tris buffered saline at pH 7.4 (TBS) then incubated overnight at 4° C in TBS with 5% normal goat serum (NGS) and 1.25% Triton X-100. Next, the sections were rinsed in TBS and then incubated in the ABC solution for 4 hours at room temperature. The sections were then rinsed with TBS and incubated in a 0.05% solution of 3, 3’ diaminobenzidine tetrahydrochloride (DAB) (08980681, MP Biochemicals, Ohio) for approximately 10 minutes. Subsequently, 30% hydrogen peroxide (H_2O_2) was added to the DAB solution achieving a final H_2O_2 concentration of 0.012%. The tissue was incubated in the DAB/H_2O_2 solution for another 8-10 minutes yielding an insoluble brown reaction product and immediately placed in TBS to stop the reaction. Following this processing, the BDA stained tissue sections were then rinsed in TBS, mounted on subbed slides, dried, then dehydrated in graded alcohol solutions, cleared in xylene and coverslipped using Permount.

Next, an additional separate series of tissue sections was used for double labeling in which both BDA and LYD (or BDA and FD) were visualized employing a simple multiple colorimetric detection method. To accomplish this, BDA was reacted first in a full series of tissue sections according to the above ABC labeling protocol staining BDA brown with DAB. The same tissue sections were then rinsed in TBS and incubated in TBS with 5% NGS and 1.25% Triton X-100 overnight. The tissue sections were then transferred and incubated in 5% goat serum in TBS with biotinylated anti-lucifer yellow directed against LYD at a dilution of 1:200, A5751, Molecular Probes, Eugene, OR) or biotinylated anti fluorescein directed against FD at a dilution of 1:500, BA-0601, Vector Laboratories) for approximately 40 hours at 4° C. The tissue was then rinsed in TBS and incubated in a solution of ABC for 4 hours at room temperature, rinsed again in TBS and incubated with the Vector SG peroxidase substrate kit (SK-4700, Vector laboratories) for approximately 5-10 minutes yielding a blue reaction product for the second tracer (LYD or FD). The sections were rinsed, mounted on subbed glass slides, dried, dehydrated and coverslipped using Permount. Thus, BDA was stained brown and LYD or FD was stained blue in the same tissue sections (Figs. 2A-F, 3D-F). Finally, in 2 additional animals that did not receive motor

cortex injections, we studied NeuN stained spinal cord sections to assist in the analysis of identifying Rexed' laminae (Morecraft et al., 2013, see Fig. 5). The NeuN immunohistochemical and tissue processing procedures that were followed have been provided in our previous reports (Morecraft et al., 2013; Morecraft et al., 2012).

Data Analysis

Localization of the cortical injection site and the terminal boutons within the spinal gray matter (C5-T1) was accomplished using brightfield illumination on a BX-51 Olympus microscope (Leeds Precision Instruments, Minneapolis, MN). Attached to the microscope was a high resolution MAC 5000 motorized stage (Ludl Electronic Products, Hawthorne, NY, USA) which was joined to the Neurolucida (RRID:SCR_001775) and Stereo Investigator (RRID:_SCR002526) neuroanatomical data collection software (Microbrightfield, Inc., (RRID:_SCR_004314), Colchester, VT, USA) in a Dell Precision Tower 5810. The Neurolucida system was used to plot the major anatomical structures and their boundaries in Nissl and immunohistochemical stained tissue sections and record the locations of the cortical injection site and distribution of terminallike profiles (boutons) in the spinal cord in immunohistochemically processed tissue sections.

The cortical injection sites in LPMC were localized by plotting the external boundary of the core region and external boundary of the halo region. The core region of the injection site was defined as the location of dense immunohistochemically reaction product characterized microscopically by a dense brown-black appearance in BDA sections and a dense blue-black appearance in LYD or FD material obscuring cellular detail of the gray matter (Mesulam, 1982). The zone characterized as internal limit of the halo was defined within the limits of the gray matter (i.e., from layer I to the bottom of layer VI) where the dense precipitate that characterized the core zone diminished. The external limit of the halo was defined where small grains of reaction product were lightly interspersed among anterogradely labeled axons and terminal boutons, and well-defined retrogradely labeled cell bodies. The external limits of both the injection site core and halo were determined by mutual agreement from 2 observers (RJM and JG). Matching Nissl stained tissue sections were used to assist in the cytoarchitectonic and laminar analysis of the cortex containing the injection site. The cytoarchitectonic location of each injection was determined using the Nissl based criteria and maps of the lateral premotor cortex according to and Pandya and colleagues (Morecraft, Stilwell-Morecraft, Ge, Cipolloni, & Pandya, 2015; Pandya et al., 2015). Briefly, LPMCd was subdivided into a caudal area 6DC and rostral area 6DR. These areas roughly correspond to areas F2 and F7 respectively of Matelli and colleagues as determined with cytochrome oxidase staining (Matelli, Luppino, & Rizzolatti, 1985). LPMCv was divided into a dorsal area 6Va and a ventral area 6Vb. The ventral premotor region can also be appreciated in a rostral and caudal dimension with Nissl staining (6Vr and 6Vc respectively) (Pandya et al., 2015; Petrides & Pandya, 2009) and based upon cytochrome oxidase staining (F5 rostrally and F4 caudally) (Matelli et al., 1985). However, for the present report dorsal (6Va) and ventral (6Vb) areas are recognized as all LPMCv injections were placed dorsally.

Using immunohistochemically processed spinal cord sections, terminal boutons were plotted in every other tissue section to obtain a general characterization of the topography and

relative density of the projection in Rexed's laminae with the aid of Olympus UPlanApo 20x-40x microscope objectives (Leeds Precision Instruments, Minneapolis, MN) (Figs., 4,5). Matching Nissl stained sections were used to define laminar gray matter compartmentalization within each tissue section as well as determine the segmental level boundaries within the longitudinal series of tissue sections. As detailed in our previous report, most of Rexed's laminae on both sides of the spinal cord were subdivided (Morecraft et al., 2013). Specifically, laminae I-VI were divided into medial and lateral subsectors, lamina VII into dorsolateral, dorsomedial, ventrolateral, ventromedial and ventral subsectors and lamina IX was divided into quadrants (Figs., 4, 5). Lamina X was divided into a contralateral and ipsilateral half, lamina VIII was not subdivided, and a reticulated marginal border (RMB) was recognized on both sides of the spinal cord. The RMB is an area identified by Rexed (Rexed, 1954) and Kuypers (Kuypers, 1981) as possessing extensive dendritic arbors of neurons located in the lateral part of laminae V-VII which protrude into the dorsolateral funiculus. This area also corresponds to the location noted by Kuypers to contain "spinal border cells" (sbc) of the propriospinal system (see Figs 1, 3 in Molenaar and Kuypers, 1977).

Stereological Data Analysis

Using Stereo Investigator 7 (MicroBrightField, Inc., (RRID:SCR_001775, RRID:_002526), Williston VT, USA), unbiased estimates of terminal boutons were obtained in the spinal gray matter ROI's using the 3-D Optical Fractionator probe as previously described (McNeal et al., 2010; Morecraft et al., 2013; Morecraft, McNeal, Stilwell-Morecraft, Gedney, et al., 2007) and our estimation of the cortical injection site volume (halo and core) was achieved by applying the Cavalieri probe as previously reported (Morecraft et al., 2013; Pizzimenti et al., 2007). Stereology was applied in every other tissue section through each series of cortical (injection site volume estimation) and spinal cord (terminal bouton number estimation) tissue sections. For terminal bouton estimation, unbiased sampling was applied such that each location along the tissue section axis had an equal probability of being included in the sample and all locations in the plane of section (excluding the set guard zones) had an equal probability of being sampled with the probe (Gundersen, 1986; Napper, 2018; West, 2012; West, Slomianka, & Gundersen, 1991). Counting rules were also applied across all case material so that all boutons had equal probabilities of being counted. The use of the applied 3-D probe avoids sampling biases and the most important feature of these probes is that they are not affected by variations in size, shape, orientation and distribution of the biological structures/particles of interest (Olesen, Needham, & Pakkenberg, 2017; West, 2012). Therefore, the fact that the CSP is randomly distributed throughout the laminae did not have affect the estimation process of total bouton number. The design of our stereological application (e.g., bouton definition, choice of dissector probe for quantifying bouton numbers and injection site volumes, counting frame size, guard zone depth, etc.) and technical issues related to our use of multiple dextran tracers and experimental strategies have been discussed in great detail in our previous papers (Darling et al., 2018; McNeal et al., 2010; Morecraft, Ge, et al., 2015; Morecraft et al., 2016; Morecraft et al., 2013; Morecraft et al., 2018; Morecraft, McNeal, Stilwell-Morecraft, Gedney, et al., 2007).

In all cases, microscopic identification of all boutons and injection volumes was accomplished using an Olympus PlanApo 100x oil objective (Leeds Precision Instruments, Minneapolis, MN). For counting terminal boutons, the main stereological parameters included the counting brick dimensions, tissue thickness, counting brick placement, guard zones and dissector height. The same counting frame (109.2/71.4 μm) and X/Y grid placement (125.3/241.9 μm) was applied to all case material as in our previous CSP reports on M1 and M2 (McNeal et al., 2010; Morecraft et al., 2013). Tissue thickness was determined by sampling 5 random gray matter sites in every other section then computing an average from this data.

In the spinal cord we estimated bouton numbers in all of Rexed's lamina (and respective subcompartments, Morecraft et al., 2013). In addition, we conducted a contralateral and ipsilateral segmental analysis for total bouton number at each segmental level (C5, C6, C7, C8 and T1) and performed a segmental analysis for terminal boutons in contralateral laminae VII and IX for all cases. Finally, we also performed a bilateral segmental analysis for the lamina VIII CSP in one key experimental case that demonstrated a very strong and consistent CSP to lamina VIII.

Data Reconstruction and Presentation

Publication quality images of injection sites, labeled fibers and labeled boutons were captured using a Spotflex 64 Mp shifting pixel camera, (Diagnostic Instruments Inc., Sterling Heights, MI, USA, version 4.6), mounted on an Olympus BX51 microscope. Photographic montages of the injection sites and labeled fibers were created using Adobe Photoshop 7.0 (Adobe Systems Inc., San Jose, CA, USA) (Figs., 2, 3). Brightness and contrast were adjusted in the images. Cortical reconstructions were developed as previously described using metrically calibrated digital images of the cortical surface (Morecraft & Van Hoesen, 1992). Publication quality illustrations were created using Adobe Illustrator and Adobe Photoshop (Adobe Systems Inc., San Jose, CA, USA) (e.g., Figs, 1, 4, 5).

RESULTS

Histological analysis of all 9 cortical injection sites revealed that all tracer injection sites were confined to the lateral premotor cortex region and in no case did the injection site spread inferiorly to involve subcortical gray matter structures. All injection sites involved layer V of area 6 which harbors pyramidal cells that give rise to corticospinal projections (H. G. J. M. Kuypers, 1981). The dorsolateral motor and premotor regions were evaluated for cytoarchitecture according to the criteria of Pandya and colleagues (Morecraft et al., 2012; Morecraft, Stilwell-Morecraft, et al., 2015; Pandya et al., 2015). Specifically, the cytoarchitectural organization (areas 4, 6DC, 6DR, 6Va, and 6Vb) was microscopically determined and superimposed on the reconstructed injection site location (Fig. 1, see gray lines). Our ICMS maps were consulted to assist in defining the border between LPMC/area 6 and M1/ area 4, as stimulation thresholds are generally higher in LPMC/area 6.

All LPMCd injection sites involved cytoarchitectonic area 6DC (Fig. 1). A very small portion of the LPMCd injection site in cases SDM54-BDA, SDM61-FD and SDM72-LYD also involved the caudal region of architectonic area 6DR. In case SDM77, in addition to

area 6DC involvement, the injection site occupied the rostral most part of adjacent area 4. LPMCv injection site cases SDM57-BDA and SDM61-BDA were largely confined to the lateral/gyral surface of the dorsal LPMCv region, corresponding to architectonic area 6Va, with minimal tracer involvement (i.e., halo) of cortex lining the posterior bank of the inferior limb of the arcuate sulcus. In LPMCv case SDM72-FD, the injection site also involved the gyral/surface region corresponding to architectonic area 6Va. However, fairly extensive involvement of the cortex lining the caudal bank of the upper part of the inferior limb of the arcuate sulcus occurred (Fig. 3D). Cytoarchitectonically this cortical field is also designated as part of sulcal area 6Va (which corresponds to area F5p of Borra et al., 2010).

LPMCd CSP to C5-T1

In our previous study examining the CSP from the M1 arm/hand area, the injection sites were of the same volume of tracer and placed in an equivalent cortical location, centered dorsoventrally within the ICMS determined arm/hand region and within the cortex lining the anterior bank of the central sulcus and adjacent gyral operculum (Morecraft et al., 2013). This allowed us to compute an average total bouton number amongst the cases in the various subsectors of Rexed's lamina to obtain a general overview of this M1 CSP. However, in the current report all injection sites were located in a slightly different cortical location of LPMCd, with some notable overlap based upon surface reconstruction and cytoarchitectonic analysis. Therefore, in this report we present each case individually. The results from case SDM57-FD are described first as the CSP observations were most representative due to the injection site involving a significant portion of the inferior part of area 6DC (Fig. 1), and corresponding to a location that has been shown to harbor the highest density of LPMCd corticospinal projection neurons following retrograde tracer placed into the cervical enlargement (Dum & Strick, 1991; Galea & Darian-Smith, 1994; He et al., 1993). This description is followed by a report of the findings from the LPMCd injection sites in cases SDM61-FD and SDM54-BDA. Finally, we describe the outcome of experimental cases SDM72-BDA and SDM72-LYD which were designed to assess the strength (in terms of terminal bouton number) of the LPMCd CSP from the most rostral part of LPMCd known to harbor very few CSP neurons (Biber, Kneisley, & LaVail, 1978; Catsman-Berrevoets & Kuypers, 1976; Dum & Strick, 1991; Galea & Darian-Smith, 1994; He et al., 1993). In all cases the descending CSP primarily traveled in the contralateral lateral corticospinal tract (Fig. 4). Considerably fewer fibers were localized in the ipsilateral lateral corticospinal tract and very few fibers occupied the ipsilateral ventral corticospinal tract. In several cases a few labeled fibers were also noted in the contralateral ventral corticospinal tract and contralateral dorsal column region (Fig. 4, see cases SDM57-FD, SDM54-BDA).

Case SDM57-FD—The SDM57-FD injection site was located in the ventral region of LPMCd involving area 6DC (Figs. 1, 2A). Not surprisingly, this case gave rise to the strongest CSP of all the injection sites studied (35,469 contralateral boutons; 9,229 ipsilateral boutons) (Figs. 4, 6B,C; Tables 2,3). The projection was primarily contralateral (79%) with the main target being contralateral lamina VII (Fig.6A,B). Within lamina VII heavy labeling occupied all subsectors with the most concentrated distribution located in the ventromedial sector (Figs. 2B, C, 7A). The second strongest contralateral projection ended in lamina VIII (Figs. 2C, 6B). To a much lesser extent, the CSP also ended in the

contralateral RMB as well as in laminae VI and IX (Fig. 6B). In terms of topography the terminal distribution was similarly dispersed in the medial and lateral parts of lamina VI (Fig. 6B). Within contralateral lamina IX, the fibers terminated primarily in the dorsomedial quadrant and a few labeled terminals were noted in the ventromedial quadrant (Fig. 8). Finally, labeled terminals were found in the contralateral part of lamina X (Fig. 6B).

From a segmental perspective, heavy contralateral labeling occurred from C5 to C7, but the intensity of the CSP diminished at C8 and T1 (Fig. 9A). For the most part, the principal target throughout C5-T1 was the ventromedial sector of lamina VII with the exception of C6 and C7, where the projection was slightly greater in the ventrolateral and ventral sectors respectively (Fig. 10A). For the projection to lamina IX, the densest distribution occurred in the dorsomedial quadrant at C5-C7 and diminished significantly in the same location at segmental levels C8 and T1 (Fig. 10C). At T1 we also found evidence of a lamina IX projection to the ventromedial sector of lamina IX (Fig. 10C). We also performed a segmental analysis of the lamina VIII projection and found the contralateral pattern to be well distributed across all cervical enlargement segments, with a stepwise increase from levels C6 to C8 (Figure 10D).

With regard to the ipsilateral CSP, the primary targets were laminae VII and VIII (Fig. 6C). Like the contralateral CSP, the ipsilateral lamina VII projection dominantly innervated the ventromedial sector, with fewer terminals occupying the dorsomedial, ventrolateral and ventral sectors (Figs. 7B, 10B). Terminations were noted in the ipsilateral part of lamina X (Fig. 6C).

The segmental distribution of the total ipsilateral CSP revealed a relatively consistent distribution across C5 to T1, with a comparatively stronger projection to levels C5 and C6 (Fig. 9B) involving primarily the ventromedial sector of lamina VII. Our segmental analysis of lamina VIII also showed a consistent ipsilateral projection throughout C5-T1 (Fig. 10D), thus demonstrating a relatively balanced bilateral projection from caudolateral part of LPMCd to lamina VIII at all cervical enlargement levels.

CASE SDM61-FD—The SDM61-FD injection site was located in the ventral region of LPMCd involving area 6DC and a very small portion of area 6DR (Figs. 1, 2D). Comparatively, this injection site was slightly dorsal and rostral to the location of the injection site in case SDM57-FD. Consequently, the terminal density of the CSP (18,892 contralateral boutons; 7085 ipsilateral boutons) was much less than that found in case SDM57-FD (Figs. 4, 6B,C; Tables 2,3). Although the CSP in case SDM61-FD was primarily contralateral, the laterality decreased (when compared to that of case SDM57-FD) from 79.4% to 72.7% contralateral (Fig. 6A). As in case SDM57-FD, the primary site of innervation in case SDM61-FD was contralateral lamina VII, with considerably fewer labeled boutons found in laminae VI, VIII and IX and the RMB (Figs. 2E, F, 6B). Interestingly, the lamina VIII projection drastically decreased in number compared to lamina VIII projection in case SDM57-FD (Fig. 6B). The projection was distributed over all subsectors within contralateral lamina VII, with the chief target being the dorsomedial and ventromedial subsectors (Fig. 7A). The projection to lamina IX involved the dorsomedial

quadrant and to a lesser extent the dorsolateral quadrant (Fig. 8). Finally, a few labeled terminals were noted in the contralateral part of lamina X (Fig. 6B).

Segmentally, the contralateral CSP involved all segmental levels but the strongest projection ended at C5 and C6 (Fig. 9A). Within lamina VII, the projection tended to be preferentially distributed in the dorsomedial and ventromedial regions at all segmental levels with two exceptions, at C6 where the projection was primarily in the ventromedial sector and ventrolateral sector and at C7 the projection predominately involved the dorsomedial and dorsolateral regions. Terminals occupied the dorsomedial quadrant within lamina IX at C5 and C6 and some were noted in the dorsolateral region at C6 and T1.

Much like case SDM57-FD, the ipsilateral CSP involved lamina VII and VIII (Fig. 6C) with the ventromedial subsector being the primary target in lamina VII (Fig. 7B). Segmentally the ipsilateral CSP from C5 to T1 revealed a gradual decline in bouton number from cranial to caudal levels (Fig. 9B).

CASE SDM54-BDA—The SDM54-BDA injection site was located in the ventrorostral region of LPMCd, involving area 6DC and a very small portion of adjacent area 6DR (Fig. 1). Comparatively, this injection site was similar in size to the injection site in case SDM61-FD but did not involve as much of the more caudally located part of area 6DC as found in case SDM61-FD. Comparatively, the number of labeled terminals (3,776 contralateral boutons; 1,389 ipsilateral boutons) was substantially less than the total estimated CSP boutons found in case SDM61-FD (Tables 2,3). The CSP in case SDM54-BDA was also primarily contralateral, with CSP laterality (73.1% contralateral and 26.9% ipsilateral) being nearly identical to that found for case SDM61-FD (Figs. 4, 6A). Like both previous LPMCd cases, preferential spinal innervation ended in contralateral lamina VII (Figs. 2H, 6B). Within contralateral lamina VII light labeling was dispersed over all 5 subsectors, with the most concentrated distribution located within the dorsomedial and dorsolateral subsectors (Fig. 7A). The second strongest contralateral projection ended in lamina IX (Fig. 6B), involving only the dorsomedial quadrant (Figs. 2I, 8). Fewer terminals were found in the lateral part of layer VI and lamina VIII (Fig. 6B), demonstrating a trend of progressively diminished lamina VIII labeling across cases SDM57-FD, SDM61-FD and SDM-54-BDA. Finally, scattered boutons occupied the contralateral region of lamina X (Fig. 6B).

Our contralateral segmental analysis revealed all levels received input, with C5-C8 having similar terminal bouton numbers, and T1 clearly less (Fig. 9A). The primary target was lamina VII (Fig. 6B) but no distinct reoccurring pattern of labeling was noted. For example, at segmental level C5 all subsectors received weak input, at C6 only the dorsomedial subsector contained labeling, at C7 and T1 only the dorsolateral sector was involved, and at C8 terminals were found in all subsectors with the exception of the dorsomedial subsector. Only segmental levels C6, C7 and C8 received a contralateral projection to lamina IX, which was strongest at segmental level C7. As noted above, only the dorsomedial quadrant received input (Fig. 8).

The ipsilateral projection from case SDM54-BDA was weak involving only lamina VII and VIII (Fig. 6C). Within lamina VII labeling occupied the ventromedial and ventral sectors.

From a segmental perspective, labeling was primarily located at C5 and C6 with fewer boutons found at levels C7 and C8 and none at T1 (Fig. 9B).

CASES SDM72-BDA and SDM72-LYD—As noted, the injection site in case SDM72-BDA was located in area 6DC whereas the injection in case SDM72-LYD was placed in a more rostral location involving in part, both areas 6DC and 6DR (Fig. 1). Additionally, there was some overlap between the 2 injection sites (Fig. 1). As mentioned, both injection sites were placed in part of LPMCd, which according to retrograde studies examining the origin of corticospinal projections to the cervical enlargement, contains few corticospinal projection neurons. The results of both experiments validated the findings of these previous reports. For example, both cases gave rise to an extremely sparse contralateral projection (SDM72-BDA, 812 boutons; SDM72-LYD, 464 boutons) that was only found in lamina VII (Figs 6A, B, 7A, 8; Tables 2, 3). Within contralateral lamina VII the dorsomedial and ventral subsectors contained boutons in both cases and the dorsolateral and ventromedial sectors only in case SDM72-BDA (Fig. 7A). Segmentally, light labeling in contralateral lamina VII was found from C5-C8 in case SDM72-BDA but only at C5 in case SDM77-LYD (Fig. 9A).

SDM72-BDA demonstrated a detectable ipsilateral projection (232 boutons) but the stereology probe did not detect ipsilateral boutons in case SDM72-LYD (Fig. 6A,C; Tables 2,3). The extremely weak ipsilateral projection from case SDM72-BDA involved lamina VII and VIII (Fig. 6C). Within lamina VII only the dorsomedial sector received input. From a segmental perspective, labeling occurred only at C5 (Fig. 9B).

M1/LPMCd CSP to C5-T1

One injection site (SDM77-BDA) was evaluated for projections to the spinal cervical enlargement from the transitional region located between the caudal most part of area 6DC (caudal LPMCd) and rostral most part of area 4 (rostral M1). Unlike the other cases in this study which received 3 injections of tracer totaling 1.2μL of tracer volume, this case received only 2 injections totaling 0.8μL of tracer (Table 1).

CASE SDM77-BDA—The size of the injection site in case SDM77-BDA was small and positioned in the very caudal part of LPMCd, corresponding to the very caudal region of architectonic area 6DC (Figs. 1, 3A). Some of this injection site involved cortex corresponding to the rostral part of area 4/M1. As noted, this experiment was designed to provide insight into a possible shift in laterality that was opposite the trend observed for the major LPMCd cases SDM57-FD, SDM61-FD and SDM-54-BDA. The CSP from case SDM77-BDA was found to be 87.1% contralateral demonstrating a progressive shift toward a strong contralateral preference (Fig. 11A; Tables 4, 5). Indeed, this would be predicted since we found the CSP from the M1 arm/hand lining the anterior bank of the central sulcus, which is extremely caudal to the SDM77-BDA injection location, to be 98% contralateral (Morecraft et al., 2013).

Like all other cases, a particularly dense projection ended in contralateral lamina VII, followed by a comparatively moderate CSP to contralateral laminae VIII and IX (Figs. 3B, C, 11B). Few boutons were observed in contralateral lamina VI and the RMB ((Figs. 3F, 11B). In terms of topography all contralateral subsectors of lamina VII received a projection.

However, contrary to the medial lamina VII preference of the other LPMCd experiments, this lamina VII projection was densest laterally, with the largest number of boutons located within the ventrolateral sectors of lamina VII (Fig. 12A), providing evidence of a topographic shift toward dorsolateral intermediate zone, characteristically exhibited by the M1 arm/hand CSP (Morecraft et al., 2013). The projection was allocated in the dorsomedial and dorsolateral quadrants of contralateral lamina IX (Figs. 3C, 13), again similar to the lamina IX CSP pattern for M1 at C5-C7. The contralateral lamina VI projection involved both medial and lateral regions (Fig. 11B). Finally, a few labeled terminals were located in the contralateral half of lamina X (Fig.11B).

Our segmental analysis revealed that all contralateral brachial levels received similar levels of terminal input (Fig. 14A). Within lamina VII, no specific segmental trend was noted for anatomical subsector labeling. For example, at all levels all subsectors contained labeled boutons except the ventral subsector at C7 and the dorsomedial sector at C8. The ventrolateral subsector was the primary target at C5-C6, the ventromedial subsector at C7, the ventral sector at C8, and the dorsomedial subsector at T1. Interestingly, segmental labeling in lamina IX shifted in this experimental case to occupy only the lower levels of the cervical enlargement including C7, C8 and T1, with most terminal labeling occurring at C8 and T1. Furthermore, labeling was confined to the dorsolateral and dorsomedial quadrants. Once more, this lamina IX distribution pattern reflected a progressive shift away from the LPMCd profile, to a distal upper extremity innervation arrangement, as observed for M1 (Morecraft et al., 2013).

The ipsilateral projection from case SDM77-BDA was weak involving only lamina VII, VIII and X (Fig. 11C; Table 5). Labeling occupied the ventromedial and ventral sectors of ipsilateral lamina VII (Fig. 12B). From a segmental perspective, labeling was primarily located at C5 with fewer boutons found at levels C6 to C8, and none in ipsilateral T1 (Fig. 14B).

LPMCv CSP to C5-T1

Three injection sites (SDM57-BDA, SDM61-BDA and SDM72-FD) were evaluated for projections to the spinal cervical enlargement (Fig. 1, 3D, G). In all cases excellent dextran transport was traced caudally from the pyramidal decussation of the medulla and into the upper spinal cord region (Fig. 3H). In cases SDM57-BDA and SDM61-BDA the injection site was confined to the convexity (lateral surface) of LPMCv, and labeled axons and terminals were found only at cervical levels C1 and C2 (Fig. 3I). However, in case SDM72-FD labeled terminals were found at C5-T1 (as well as C1-C4). In this case, the descending CSP primarily traveled in the contralateral lateral corticospinal tract (Fig. 5). Considerably fewer fibers were localized in the ipsilateral lateral corticospinal tract and ipsilateral ventral corticospinal tract. The main difference between case SDM72-FD and the other 2 LPMCv cases was the injection site involved the cortex lining the posterior bank of the upper region of the inferior limb of the arcuate sulcus (area F5r of Borra et al., 2010), in addition to the gyral/lateral surface (Fig. 3D). Thus, the findings from Case SDM72-FD will be presented below.

CASE SDM72-FD—Our stereological analysis of case SDM72-FD through spinal levels C5 to T1 demonstrated a bilateral (69.6% contralateral) CSP as found for the LPMCd CSP (Figs. 5,11A; Tables 4, 5). However, in comparison, the LPMCv CSP was considerably weaker than the LPMCd CSP in cases SDM57-FD and SDM61-FD (Tables 2, 3). Like these cases however, the primary LPMCv terminal target was contralateral lamina VII of the intermediate zone (Figs. 3F, 11B). Specifically, labeled terminals were found in all of contralateral lamina VII subsectors, with the highest concentration of terminations forming a diagonal pattern involving the dorsolateral and ventromedial sectors (Figs. 5, 12B). The contralateral reticulated marginal border, lamina VIII and the lateral part of lamina VI received a comparatively moderate level of input (Figs. 3E, F, 11B). Relatively fewer labeled boutons were found in the lateral part of lamina V and contralateral half of lamina X of the central canal region (Fig. 11B). No terminal projection was found to motoneuron lamina IX (Fig. 13). Segmentally the contralateral CSP involved all spinal levels, with most boutons located at C5-C7 (Fig. 14). Within lamina VII the contralateral projection involved the dorsolateral and ventromedial region at all levels (Fig. 15A).

The ipsilateral projection from case SDM72-FD was also very sparse, equally involving lamina VII and VIII (Fig. 11C). Within lamina VII, labeling occupied the ventromedial and ventral sectors and to a lesser extent the dorsomedial region (Fig. 12B). From a segmental perspective, ipsilateral labeling was found at C5-7 with no boutons at levels C8 and T1 (Figs. 14B, 15B).

DISCUSSION

The experimental findings of the present study demonstrate that a bilateral corticospinal projection to the cervical enlargement (C5-T1) originates from the dorsolateral premotor cortex (LPMCd). The bilateral LPMCd projection is directed primarily to the medial part of lamina VII (dorsomedial, ventromedial and ventral sectors) and adjacent lamina VIII (Fig. 16A). The LPMCd CSP is additionally characterized by dense contralateral terminal labeling ending in the lateral part of lamina VII (dorsolateral and ventrolateral sectors) and a less prominent contralateral projection to lamina IX. The contralateral lamina IX projection was topographically selective, targeting the dorsomedial quadrant of lamina IX.

Evidence for two distinct LPMCd segmental innervation patterns was found. The contralateral LPMCd CSP to laminae VII and IX preferentially innervates proximal limb spinal segments C5, C6 and C7 of the cervical enlargement (Figs. 9, 10C). Fiber terminals from LPMCd to lamina VIII, noted for proximal limb and axial motor control, were distributed bilaterally throughout all levels of the enlargement, including C8 and T1 which is conventionally recognized for mediating distal, hand/digit motor control (Fig. 10D).

Several LPMCd connectional trends were isolated in our experiments. The strongest CSP to the cervical enlargement arose from the ventrocaudal part of LPMCd, corresponding to the ventrocaudal part of cytoarchitectonic area 6DC (case SDM57-FD) (Figs. 1, 6B). From this location, a gradual decline in the total number of CSP terminals occurred, progressing rostral within LPMCd/area 6DC. This caudal to rostral decline in terminal bouton labeling included a shift in laterality from a relatively dominant contralateral projection arising from the

caudal part of LPMCd and rostral part of area 4 (87%; SDM77-BDA) to a less dominant contralateral projection from the rostral part of LPMCd (72-73%; cases SDM61-FD and SDM54-BDA) (Figs., 6A, 11A). We also found a substantial bilateral CSP to lamina VIII from the ventrocaudal part of area LPMCd/area 6DC (SDM57-FD, Fig. 10D). The lamina VIII projection diminished abruptly in terminal strength progressing either caudal, or rostral to this location, and was absent ventral to this location (i.e., the convexity/lateral part of dorsal LPMCv which did not project below C2). Thus, a robust bilateral CSP from LPMCd to lamina VIII is restricted to a highly localized region of LPMCd. In contrast, the observed CSP to contralateral lamina IX was less extensive and was similar in bouton number from rostral to caudal levels of ventral LPMCd (see cases SDM57-FD and SDM-61-FD; Fig. 6B; Table 2).

The CSP to the cervical enlargement from LPMCv (SDM72-FD) originated from the post-arcuate sulcus region and was considerably weaker than the LPMCd CSP (Fig. 16B). This LPMCv CSP was bilateral, and primarily innervated the dorsolateral and ventromedial sectors of contralateral lamina VII with most terminations occurring at C5-C7 (Figs, 11A, 12B, 15A). The convexity portion of LPMCv, located on the lateral cortical surface, did not innervate spinal segmental levels below C2.

Anatomical Findings and Previous LPMCd Corticospinal Observations.

Prior to our report, only two studies systematically investigated the terminal organization of the CSP from the dorsolateral premotor cortical region in monkey (Hoff, 1935; Kuypers & Brinkman, 1970). Our findings support the general observations of Hoff by showing terminals occur primarily in the intermediate zone (Hoff, 1935) and are consistent with the more detailed observations of the Kuypers and Brinkman account (Kuypers & Brinkman, 1970) by showing that the LPMCd projection is bilateral with a concentration of terminals ending in the medial part of lamina VII including adjacent lamina VIII. Our findings further demonstrate that the ventral sector of lamina VII, located between laminae VIII and IX, receives substantial bilateral terminal input. We unequivocally show a particularly dense contralateral projection to the lateral region of lamina VII, as cautiously noted by Kuypers and Brinkman. Indeed, with the degeneration axon tracing technique it was not possible to differentiate with certainty, elements of axons en passant from axon terminals in densely labeled CNS regions, such as the lateral part of lamina VII in this circumstance (Fig. 2B, see arrows). Our findings further show that a projection to lamina IX occurs as reported by Kuypers and Brinkman, but this selectively involves the dorsomedial region of lamina IX (Fig. 8). As noted, we also found some rostral to caudal LPMCd terminal trends, and some specific segmental innervation patterns of the LPMCd CSP that were not previously reported.

Studies examining the origin of corticospinal neurons following retrograde tracers placed in the cervical enlargement of the spinal cord (C5-T1) show a particularly dense distribution of corticospinal projection neurons reside in the ventral and caudal region of LPMCd (Biber et al., 1978; Dum & Strick, 1991; Galea & Darian-Smith, 1994; He et al., 1993). This location corresponds to where we found the strongest LPMCd CSP (case SDM57-FD). The retrograde studies with injections involving both upper (C1-C4) and lower (C5-T1) cervical

levels provide evidence showing that the number of corticospinal neurons significantly decline rostral to this location (Biber et al., 1978; Dum & Strick, 1991; Galea & Darian-Smith, 1994; He et al., 1993; Nudo & Masterton, 1990; Rozzi et al., 2006; Toyoshima & Sakai, 1982). Our findings coincide with these observations as we identified a progressive decline in the number of cortiocospinal terminals from injection sites located at increasingly more rostral levels of LPMCd (see cases SDM57-FD, SDM61-FD, SDM54-BDA, and SDM72 respectively; Fig. 6B).

Anatomical Findings and Previous LPMCv Corticospinal Observations.—Our experimental findings demonstrate that the dorsal part of LPMCv residing on the lateral surface projects to the upper cervical spinal cord, but not to segmental levels below C2 (Fig. 3I). These represent the first anterograde experiments aimed to evaluate this projection from the lateral surface using high-resolution dextran tract tracers. This observation parallels findings from retrograde transport studies showing corticospinal projection neurons in this location of LPMCv following retrograde tracers injected into upper cervical levels of the spinal cord (e.g., C1-C4) (Catsman-Berrevoets & Kuypers, 1976; Dum & Strick, 1991; Martino & Strick, 1987; Nudo & Masterton, 1990; Rozzi et al., 2006; Toyoshima & Sakai, 1982), but not following injections placed at spinal levels below C5 (Dum & Strick, 1991; Galea & Darian-Smith, 1994; He et al., 1993). Our findings further suggest the caudal extent of the gyral/convexity LPMCv CSP, demonstrating that the projection ends at C2.

It is important to recognize that a recent study using anterograde dextran tracers has demonstrated a CSP to C5-T1 which originates from the dorsal and rostral-most part of LPMCv that includes the cortex lining the posterior bank of the inferior limb of the arcuate sulcus (sulcal area 6Va, or area F5r of Borra et al., 2010). One of our LPMCv injection sites (SDM72-FD) significantly involved this cortex and our findings are in excellent agreement with those of Borra and colleagues. For example, both studies found very light contralateral terminal labeling at C5-T1 that occurred primarily the contralateral lamina VII with no labeling in lamina IX. Within lamina VII, both reports show preferential innervation of the dorsolateral and ventromedial regions of lamina VII (C5-T1 in our report and at C5, C8 and T1 in Borra et al, 2010). We also confirmed the contralateral projection to lamina V and VI noted in the Borra paper. Our findings add to our understanding of this LPMCv CSP on several accounts. The contralateral projection to laminae V and VI preferentially targets the lateral region of these laminae. We present evidence for an LPMCv CSP to contralateral lamina VIII, and contralateral part of lamina X. There is a weak ipsilateral CSP that involves laminae VII and VIII and ipsilateral side of lamina X. Topographically, the ipsilateral lamina VII CSP is distributed in the ventromedial and ventral sectors. Lastly, the quantitative segmental analysis presented here further demonstrates that the contralateral CSP to the cervical enlargement, although very weak, preferentially innervates levels C5-C7.

In further support of this LPMCv projection, the upper part of the caudal bank of the arcuate sulcus inferior limb and adjacent region of the arcuate spur has been found to harbor retrogradely labeled neurons following tracer injections into C5-T1 (Dum & Strick, 1991; Galea & Darian-Smith, 1994; He et al., 1993). Together, these observations suggest that the convexity/lateral surface of LPMCv sends terminal projections only to upper cervical levels

(C1-C2) whereas a small post-arcuate portion of LPMCv weakly innervates spinal levels C5 to T1 (Fig. 16B).

Terminal Density of the M1, M2, LPMCd and LPMCv Corticospinal Projection— In two previous reports, we quantitatively described the terminal organization of the corticospinal projection to C5-T1 from the primary motor cortex (M1) (Morecraft et al., 2013) and supplementary motor cortex (M2, SMC, MII; also recognized as supplementary motor area, SMA) (McNeal et al., 2010) using multiple control cases in each report. In these studies we employed an identical experimental tract tracing paradigm and stereological design as applied in the present study investigating the LPMCd CSP for cases SDM54-BDA, SDM57-FD and SDM61-FD and LPMCv from case SDM72-FD (Table 1). Given the similarities in technical procedures and experimental parameters, our data suggest that significant differences occur in corticospinal laterality, and a connectional/anatomical hierarchy exists relative to the strength/total bouton number of corticospinal terminals arising from each major motor area.

With regard to laterality, the CSP to the cervical enlargement from LPMCd appears to be strikingly similar to what we found for M2. For example, from an average of 4 M2 control monkey cases we observed 81% of terminal boutons were located contralaterally at C5-T1 (McNeal et al., 2010). Similarly, we found 79% of labeled terminals were located contralaterally in case SDM57-FD, which gave rise to the most prominent LPMCd CSP. As pointed out, rostrally in LPMCd the CSP is approximately 73% contralateral. Collectively, these findings demonstrate that the “premotor cortex” CSP is bilateral. In significant contrast, and based upon an average of 3 M1 CSP monkey cases, the terminal distribution of the CSP from the caudal part of M1 (i.e., cortex lining the anterior bank of the central sulcus) is a dominate 98% contralateral (Morecraft et al., 2013). It will be of considerable interest to determine the laterality of the CSP from the rostral region of M1 (or “old” M1 according to Rathelot & Strick, 2009). Indeed, this cortex is positioned between LPMCd proper and caudal (or “new”) M1 which lines the anterior bank of the central sulcus. Our current findings on the laterality of the CSP from injection case SDM77-BDA (87% contralateral), which was located within the transitional region between LPMCd/area 6DC and rostral M1/area 4, suggests a gradual trend may occur through “old” M1 characterized by a slightly greater contralateral CSP progressing toward “new” M1.

In terms of total bouton number and general density, it is clear that the strongest/densest contralateral terminal CSP to the cervical enlargement (C5-T1) originates from M1 (Morecraft et al., 2013- Table 2, average = 199,214 boutons). This is followed by the contralateral terminal CSP from M2 (McNeal et al., 2010- Table 2, average = 75,853 boutons), LPMCd (Table 1, SDM57-FD = 35,469 boutons) and LPMCv (Table 4, SDM72-FD = 6,162). Correspondingly, this trend was notable for the contralateral projection to motoneuron lamina IX and propriospinal lamina VII, with significantly more corticospinal terminals occurring in both laminae from M1, followed by M2 then LPMCd. No lamina IX projection was found for LPMCv. These observations parallel the retrograde transport findings of Galea and Darian-Smith (Galea & Darian-Smith, 1994) who found the largest number of contralateral corticospinal neurons reside in M1 following injections of retrograde tracer into the cervical enlargement. They reported that the second highest

number of contralateral corticospinal neurons were located in M2 (identified as area F3/SMA/mesial area 6aα in the Galea and Darian-Smith paper) followed by comparatively less corticospinal neurons located in LPMCd (identified as area F2/dorsolateral area 6aα in the Galea and Darian-Smith paper) and fewest in the region of the arcuate spur/inferior arcuate sulcus (identified as the post-arcuate area).

Interestingly we found the inverse relationship to occur for the contralateral terminal projection to lamina VIII. The highest number of corticospinal terminations in lamina VIII resulted from injections of dextran tracer into LPMCd (case SDM57-FD), followed by M2 (McNeal et al., 2010), and then M1 which had the fewest number of contralateral terminations in lamina VIII (Morecraft et al., 2013).

Kuypers' Proximal Motor Control System and Woolsey's Axial Representation—In addition to gaining contemporary insight into the anatomical organization of the LPMCd corticospinal projection, our experimental plan was designed to re-examine Kuypers' conceptualization of the descending medial motor control system, which he proposed was organized to control postural and proximal limb movements (Kuypers & Brinkman, 1970; Kuypers, 1982; Lawrence & Kuypers, 1968, - for review see Lemon, 2008a, 2008b; Lemon, Landau, Tutssel, & Lawrence, 2012). Our findings provide substantial support for the medial motor system model from the perspective of the LPMCd CSP to the spinal intermediate zone (lamina VII). Consistent with Kuypers and Brinkman (1970) observations, we found powerful bilateral corticospinal terminations ending in the medial region of lamina VII and adjacent lamina VIII (Fig. 16A, see area identified in red). Notably, lamina VIII contains motoneurons innervating axial musculature via dorsal primary rami (Sprague, 1948). In addition, propriospinal neurons located in both spinal regions (medial lamina VII and lamina VIII) give rise to long, bilateral intraspinal axon projections (Matsushita, Ikeda, & Hosoya, 1979; Molenaar & Kuypers, 1978) that ascend and descend in the ventral funiculi. These projections issue frequent collaterals that re-enter the gray matter to terminate on motoneurons of proximal extremity muscles and axial muscles (Matsushita et al., 1979; Molenaar, 1978; Molenaar & Kuypers, 1978; Molenaar, Rustioni, & Kuypers, 1974; Rustioni, Kuypers, & Holstege, 1971; Sterling & Kuypers, 1968 – see Kuypers, 1982 for review). Overall, there is good reason to believe that this circuitry is well-structured to govern movements of the girdle/proximal limb and axial/vertebral region, and as such contribute to neural systems implicated in postural control and reaching.

The observations of the present study extend Kuypers medial motor system concept in several notable ways. First was our finding of a topographically specific contralateral LPMCd CSP to the dorsomedial quadrant of lamina IX which is known to harbor proximal upper limb flexor motoneurons (Jenny & Inukai, 1983; Reed, 1940). This would suggest potential involvement in control of reaching. Second, complimenting this observation we found the contralateral LPMCd CSP to laminae VII and IX preferentially innervate spinal levels C5-C7, which control neck, back, shoulder and elbow movements. Third, we found a bilateral projection to lamina VIII that surprisingly involved all segmental levels of the enlargement, including levels C8 and T1 which are conventionally recognized for mediating wrist and digit movements. Based upon this evidence, it is probable that the LPMCd CSP to lamina VIII could serve to activate axial muscles locally (C5-T1) through the direct

projections to axial motoneurons, as well as at widespread vertebral levels via the CSP projection to lamina VIII propriospinal neurons. The net effect of this circuitry may be for postural stabilization accompanying simultaneous hand and digit movements mediated primarily by M1 corticospinal projections to lamina IX flexor, extensor, adductor and abductor motoneurons located at C8 and T1 (Morecraft et al., 2013).

Kuypers often acknowledged supportive physiological observations reported around the time he developed his descending medial and lateral motor system concepts. This included the findings of Clinton Woolsey, who was one of the most recognized neuroscientists in the field of cortical functional localization (Lyon et al., 2014; Thompson, 1999). One of Woolsey's most cited contributions included his surface stimulation findings of motor cortex in the pentobarbital anesthetized monkey preparation (Fig. 17A) (Woolsey et al., 1952). His observations supported the existence of one major precentral motor cortex (MI), and a second smaller motor representation, the supplementary motor cortex (MII) (Fig. 17C) (Woolsey et al., 1952; Woolsey, 1958). Although the rostral part of the precentral motor cortex (MI) was considered by many authorities to be "premotor cortex" (Fulton, 1949), Woolsey's surface stimulation work demonstrated this cortex evoked axial and proximal limb upper extremity movements. Notwithstanding the debate that followed for many decades, our present CSP findings provide a plausible explanation for what Woolsey and his colleagues observed in the surgical suite when he stimulated the ventrocaudal region of LPMCd. Careful examination of his trademark "figurines" show that cortex located just ventral and rostral to the superior precentral dimple/sulcus elicited movements in the upper (cervical) axial region, including shoulder and elbow movements (Fig. 17A, B). Our findings show if the epicortical stimulating pulse activated the LPMCd CSP as found in case SDM57-FD, which closely corresponds to this cortical location (Figs. 1, 17A see cortex outlined by the solid red line), this movement pattern is precisely what we would predict based upon the terminal pattern of the CSP presented here, and corresponding anatomical organization of the cervical spinal cord as summarized above. This would also be congruent with the intracortical microstimulation (ICMS) observations demonstrating shoulder (Kwan et al., 1978b; Raos, Umilta, Gallese, & Fogassi, 2004; Stark, Asher, & Abeles, 2007) and trunk/axial (Godschalk, Mitz, van Duin, & van der Burg, 1995) movements are evoked from this same dorsolateral premotor location. This general cortical region has also been shown to contain retrogradely labeled cells following injection of rabies virus into the spinodeltoid muscle of the rhesus monkey (Rathelot & Strick, 2009). As we will briefly discuss below, our anatomical evidence suggests that current observations of "dorsolateral premotor" contributions to grasping and manipulation cannot be a direct result of corticospinal output derived from this brain region as both Kuypers and Woolsey contended.

Additional Functional Considerations

For nearly a century, unraveling the functional contribution of LPMCd to voluntary motor behavior has been a priority of cortical motor system investigators. Early lesion studies in non-human primates demonstrated lateral premotor cortex injury alters the ability to execute complex purposeful voluntary upper extremity movements (Fulton, 1935, 1949; Jacobsen, 1934, 1935 – see Darling, Pizzimenti, & Morecraft, 2011 for review). Contemporary neurophysiological recording studies have shown that LPMCd neurons are active during the

preparation, initiation and execution phases of arm movements (see Hoshi & Tanji, 2007 for review). More recent unit recording work reported single neurons in LPMCd encode the kinematics of both reaching and grasping movements (Takahashi et al., 2017), grip type and grasp time course (Hao et al., 2014) and moderate their activity according to object dimensions and applied forces (Hendrix, Mason, & Ebner, 2009). Other current studies indicate that LPMCd neurons are active during both visually-guided and memory-guided sequential arm pointing movements but make a significant contribution only to the generation of cortically mediated memory-guided arm movement sequences (Ohbayashi, Picard, & Strick, 2016). Our findings demonstrate that the corticospinal projection from LPMCd is structured to govern axial and girdle/proximal upper limb musculature that would likely be involved in postural stabilization and perhaps, control of the proximal limb during reaching. Thus, distal upper extremity motor control contributions from LPMCd, including influence on grasping and manipulation, are likely to occur through indirect multisynapic neural networks. These might include reciprocal corticocortical projections with M1, descending LPMCd projections to subcortical targets, or through contralateral LPMCd corticospinal input to the spinal intermediate zone. This conclusion would be in agreement with stimulus triggered averaging (StTA) observations which demonstrate LPMCd short latency post-stimulus effects similar to M1 occur only in proximal upper limb muscles (shoulder and elbow), indicating direct LPMCd CSP's may terminate only on proximal limb motoneurons (Boudrias, McPherson, Frost, & Cheney, 2010). In contrast, the latency effects accompanying LPMCd stimulation on distal upper limb muscle activation was 2-3 ms longer compared to M1. Boudrias and colleagues suggested their findings supported a role for LPMCd on the reach process, which mainly involves proximal joints (Kurata & Hoffman, 1994). They also concluded that LPMCd corticospinal projections are not likely to directly affect distal upper extremity motoneurons/movements, and such an effect is likely to occur through indirect coupling, or via slow corticospinal conduction velocities (Boudrias et al., 2010).

We found that the convexity/lateral portion of LPMCv did not innervate spinal levels located below C2. This observation suggests that the CSP from the gyral/lateral portion of LPMCv may affect upper neck movement. This would support Woolsey's observations of neck movements following epicortical stimulation of ventral area 6 located directly above the orofacial representation (Fig. 17A) (Woolsey et al., 1952) and ICMS observations showing neck and axial movements can be evoked from this general LPMCv location (Gentilucci et al., 1988; Godschalk et al., 1995). Importantly, our findings also indicate that this (gyral) LPMCv CSP does not have a direct projection to the C3-C4 propriospinal relay system that is known to mediate distal upper extremity movements in the cat and monkey through C3/C4 intermediate zone projections to lamina IX motoneurons at C8 and T1 (Alstermark et al., 2011; Isa, Ohki, Seki, & Alstermark, 2006; Kinoshita et al., 2012). These experimental findings indirectly support the suggestion that LPMCv effects on distal upper extremity movements in monkey are significantly mediated through corticocortical circuits modulating corticospinal output arising from the M1 arm/hand area (Cerri, Shimazu, Maier, & Lemon, 2003; Prabhu et al., 2009; Schmidlin, Brochier, Maier, Kirkwood, & Lemon, 2008; Shimazu, Maier, Cerri, Kirkwood, & Lemon, 2004). Finally, it is possible that a potential LPMCv CSP that may reach C5-T1, as found here (Fig. 16B) and by Borra et al., (2010) in monkey, may

be structured differently in the human brain. But a recent stimulation study in humans has also shown LPMCv-M1 mediated corticocortical interconnections, or other indirect LPMCv neuronal circuits may be necessary for LPMCv influence on hand movements. Specifically, Fornia and colleagues report longer latencies to hand muscles for single (and multiple) pulse stimulation to ventrolateral premotor cortex than compared to M1 stimulation effects (Fornia et al., 2018). This work also demonstrated that higher intensity stimulation was required when stimulating LPMCv than M1, indicating lower excitability of the ventrolateral premotor region.

Potential Role of the LPMC CSP in Motor Recovery after Precentral Cortical Injury

LPMCd Corticospinal Projection and Potential Proximal Upper Limb Recovery

—Understanding the potential role of spared LPMC in motor recovery of the hand and digits following damage to M1 has received considerable attention (Baker, Zaaimi, Fisher, Edgley, & Soteropoulos, 2015; Ganguly, Byl, & Abrams, 2013; Kantak, Stinear, Buch, & Cohen, 2012; Plow, Cunningham, Varnerin, & Machado, 2015). Underlying optimism for such a role is the thought that following M1 injury, the LPMC corticospinal projection may be a target for therapeutic intervention to assist re-innervation processes of spinal cord targets that have lost M1 input, which is a common occurrence following middle cerebral artery (MCA) stroke. With respect to the LPMCd corticospinal projection, our findings indicate that this would be a formidable challenge. The main obstacle would be the topographical distribution of M1 and LPMCd CSP being vastly different with one major exception. As we have previously shown, the CSP from the arm/hand region of M1 is a nearly exclusive contralateral projection (98%). In terms of topography, M1 terminals target the dorsal and lateral sectors of lamina VII, the dorsal quadrants of motoneuron lamina IX at levels C5-C7, and all quadrants of lamina IX at C8 and T1 (Morecraft et al., 2013). In striking contrast, we found the LPMCd CSP is bilateral and primarily targets the medial and ventral sectors of lamina VII and adjacent lamina VIII. Furthermore, the projection to lamina IX innervates the dorsomedial quadrant of lamina IX, but this occurs preferentially at C5-C7, with very few terminal boutons at C8 and T1. Thus, for the LPMCd CSP to “take over” some of M1’s exquisite grasping and manipulation functions, significant axon terminal rearrangement would be required in the form of extensive sprouting into the lateral regions of lamina IX at C5 to C7, as well as caudally into spinal levels C8 and T1. However, based upon our experience in the monkey cortical lesion model, spontaneous (e.g., no therapeutic intervention) upregulation of spared supplementary motor (M2) CSP terminals following M1 hand injury occurs only in spinal cord sectors that have axon terminals as shown in controls (McNeal et al., 2010; Morecraft, Ge, et al., 2015; Morecraft et al., 2016). This would indicate LPMCd CSP proliferation may occur in spinal subsectors mediating proximal limb recovery (e.g., bilaterally in medial lamina VII and lamina VIII). In this regard, a spared LPMCd CSP appears to be in a favorable position to contribute to recovery of postural stabilization and reaching, particularly following compromise of the shoulder/trunk representation of M1 which lies caudal to LPMCd, and directly dorsal to the M1 arm/hand area (Fig. 17A, see area outlined by the dashed red line) (Boudrias et al., 2010; Darling et al., 2013; Darling et al., 2016; Hudson, Park, Belhaj-Saif, & Cheney, 2017; Kwan, Mackay, Murphy, & Wong, 1978a; Weinrich & Wise, 1982).

LPMCd and LPMCv Corticospinal Projection and Potential Distal Upper Limb Recovery—Yet there is one important exception to the problem related to distal upper limb motor recovery, and this relates to the CSP findings from both LPMCd (SDM57-FD) and the post-arcuate region of LPMCv (SDM72-FD). In the current report we found a particularly dense LPMCd CSP (SDM57-FD) to the lateral sectors of contralateral lamina VII at C5-C7, and a moderate CSP to the lateral sectors of contralateral lamina VII at C8 and T1 (Figs. 7A, 10A, 16A - see contralateral lamina VII area highlighted in blue). Similarly, we found a weak but relatively consistent LPMCv projection to the dorsolateral sector of lamina VII throughout C5-T1 (Fig. 15A). According to Kuypers motor control model, this lateral lamina VII projection would fall into the “lateral motor system” domain, which is organized to steer distal upper extremity motor function (Kuypers, 1982 – for review see Lemon, 2008b; Lemon et al., 2012). Indeed, propriospinal neurons in lateral lamina VII give rise to ipsilateral projections to motoneurons in lamina IX, including at spinal levels C8 and T1 (Sterling and Kuypers, 1968 - see their Fig. 13; Rustoni et al., 1970; Molenaar et al., 1974; Molennar, 1978; Molenaar and Kuypers, 1978; Matsushita et al., 1979 – see Kuypers, 1982 for review) which could theoretically support distal upper extremity recovery. Of note, this potential recovery scenario would not pertain to the LPMCd or LPMCv CSP originating from the non-lesioned hemisphere because the ipsilateral CSP from both premotor areas primarily innervate the dorsomedial, ventromedial and ventral subsectors of lamina VII (Figs. 7B, 10B, 12B).

As for the LPMCv CSP originating from the convexity/lateral surface, this projection did not innervate spinal levels below C2. Thus, transcranial stimulation efforts in recovering patents with M1 damage focusing on the lateral surface of the ventral premotor region may not have a direct effect on upper extremity related spinal circuitry (i.e., C3-T1) if this corticospinal projection is structured similarly in humans. As noted, this would require the LPMCv CSP to at least reach C3 and C4, where lateral lamina VII propriospinal neurons are known to innervate lamina IX motoneurons at C8 and T1 (Alstermark et al., 2011; Kinoshita et al., 2012).

Frontal versus Frontoparietal Injury—Our experience would also suggest that such corticospinal terminal proliferation may occur following isolated lateral motor cortex injury (McNeal et al., 2010; Morecraft et al., 2016), but not when the primary somatosensory cortex (S1) is incorporated into the injury scenario (Morecraft, Ge, et al., 2015). Indeed our experiments show that isolated lateral motor cortex injury (M1+LPMC) results in an upregulated corticospinal projection from spared premotor cortex (i.e., M2; (McNeal et al., 2010), but inclusion of S1 in the injury (M1+LPMC+ S1) results in degradation of corticospinal terminals from what appears to be “healthy” uninjured premotor cortex (i.e., M2; Morecraft, Ge, et al., 2015). In this case, we found corticoreticular projections proliferate from spared premotor cortex (M2) and this important upregulation of reticular input correlates with arm and hand recovery (Darling et al., 2018). Notably, increased M2 corticoreticular input did not occur following isolated lateral motor cortex injury, only enhanced M2 corticospinal projections.

Summary and Conclusions

In the rhesus monkey, the CSP from the lateral, or convexity portion of LPMCv did not project below C2 whereas the CSP from LPMCv located in the post-arcuate region sent a weak bilateral CSP to C5-T1 that ended primarily in contralateral lamina VII. In contrast, we demonstrate a strong bilateral ventromedial CSP from LPMCd to C5-T1 that is structured to influence axial and proximal upper limb movements possibly involved in postural stabilization and control of reaching. A sizeable LPMCd projection was also found to the lateral part of contralateral lamina VII. Collectively, our findings show that contributions of LPMC to grasping and manipulation are likely to be mediated through indirect neural network connections including corticocortical, subcortical or intrinsic spinal circuits. Clinically, our findings indicate that spared LPMCd CSP following MCA stroke may contribute to recovery of axial and proximal limb movements following injury to the M1 shoulder/trunk representation. It is also conceivable that the LPMC CSP may support distal upper extremity recovery following injury to the M1 arm/hand representation through indirect circuits mediated by the contralateral LPMC CSP to the lateral region of lamina VII.

Acknowledgments/GRANT SUPPORT:

National Institutes of Health, NS 097450, NS 046367; NS 33003

COMMON ABBREVIATIONS:

BDA	biotinylated dextran amine
FD	fluorescein dextran
LPMC	lateral premotor cortex
LPMCd	dorsolateral premotor cortex
LPMCv	ventrolateral premotor cortex
LYD	lucifer yellow dextran

REFERENCES

Alstermark B, Pettersson LG, Nishimura Y, Yoshino-Saito K, Tsuboi F, Takahashi M, & Isa T (2011). Motor command for precision grip in the macaque monkey can be mediated by spinal interneurons. J Neurophysiol, 106(1), 122–126. doi:10.1152/jn.00089.2011 [PubMed: 21511706]

Baker SN, Zaaimi B, Fisher KM, Edgley SA, & Soteropoulos DS (2015). Pathways mediating functional recovery. Prog Brain Res, 218, 389–412. doi:10.1016/bs.pbr.2014.12.010 [PubMed: 25890147]

Biber MP, Kneisley LW, & LaVail JH (1978). Cortical neurons projecting to the cervical and lumbar enlargements of the spinal cord in young and adult rhesus monkeys. Exp Neurol, 59(3), 492–508. [PubMed: 417943]

Borra E, Belmalih A, Gerbella M, Rozzi S, & Luppino G (2010). Projections of the hand field of the macaque ventral premotor area F5 to the brainstem and spinal cord. J Comp Neurol, 518(13), 2570–2591. doi:10.1002/cne.22353 [PubMed: 20503428]

Boudrias MH, McPherson RL, Frost SB, & Cheney PD (2010). Output properties and organization of the forelimb representation of motor areas on the lateral aspect of the hemisphere in rhesus macaques. Cereb Cortex, 20(1), 169–186. doi:10.1093/cercor/bhp084 [PubMed: 19561063]

Catsman-Berrevoets CE, & Kuypers HG (1976). Cells of origin of cortical projections to dorsal column nuclei, spinal cord and bulbar medial reticular formation in the rhesus monkey. Neurosci Lett, 3(5-6), 245–252. [PubMed: 19604894]

Cerri G, Shimazu H, Maier MA, & Lemon RN (2003). Facilitation from ventral premotor cortex of primary motor cortex outputs to macaque hand muscles. J Neurophysiol, 90(2), 832–842. doi: 10.1152/jn.01026.2002 [PubMed: 12904495]

Darling WG, Ge J, Stilwell-Morecraft KS, Rotella DL, Pizzimenti MA, & Morecraft RJ (2018). Hand Motor Recovery Following Extensive Frontoparietal Cortical Injury Is Accompanied by Upregulated Corticoreticular Projections in Monkey. J Neurosci, 38(28), 6323–6339. doi:10.1523/JNEUROSCI.0403-18.2018 [PubMed: 29899028]

Darling WG, Helle N, Pizzimenti MA, Rotella DL, Hynes SM, Ge J, … Morecraft RJ (2013). Laterality affects spontaneous recovery of contralateral hand motor function following motor cortex injury in rhesus monkeys. Exp Brain Res, 228(1), 9–24. doi:10.1007/s00221-013-3533-1 [PubMed: 23652723]

Darling WG, Pizzimenti MA, & Morecraft RJ (2011). Functional recovery following motor cortex lesions in non-human primates: experimental implications for human stroke patients. J Integr Neurosci, 10(3), 353–384. doi:10.1142/S0219635211002737 [PubMed: 21960307]

Darling WG, Pizzimenti MA, Rotella DL, Hynes SM, Ge J, Stilwell-Morecraft K, & Morecraft RJ (2016). Sensorimotor cortex injury effects on recovery of contralesional dexterous movements in Macaca mulatta. Exp Neurol, 281, 37–52. doi:10.1016/j.expneurol.2016.04.004 [PubMed: 27091225]

Dum RP, & Strick PL (1991). The origin of corticospinal projections from the premotor areas in the frontal lobe. J Neurosci, 11(3), 667–689. [PubMed: 1705965]

Fornia L, Ferpozzi V, Montagna M, Rossi M, Riva M, Pessina F, … Cerri G (2018). Functional Characterization of the Left Ventrolateral Premotor Cortex in Humans: A Direct Electrophysiological Approach. Cereb Cortex, 28(1), 167–183. doi:10.1093/cercor/bhw365 [PubMed: 27920095]

Fulton JF (1935). A note on the definition of the "motor" and "premotor" areas. London: John Bale, Sons & Danielsson.

Fulton JF (1949). Physiology of the nervous system (3d ed.). New York: Oxford University Press.

Galea MP, & Darian-Smith I (1994). Multiple corticospinal neuron populations in the macaque monkey are specified by their unique cortical origins, spinal terminations, and connections. Cereb Cortex, 4(2), 166–194. [PubMed: 8038567]

Ganguly K, Byl NN, & Abrams GM (2013). Neurorehabilitation: motor recovery after stroke as an example. Ann Neurol, 74(3), 373–381. doi:10.1002/ana.23994 [PubMed: 25813243]

Gentilucci M, Fogassi L, Luppino G, Matelli M, Camarda R, & Rizzolatti G (1988). Functional organization of inferior area 6 in the macaque monkey. I. Somatotopy and the control of proximal movements. Exp Brain Res, 71(3), 475–490. [PubMed: 3416964]

Godschalk M, Mitz AR, van Duin B, & van der Burg H (1995). Somatotopy of monkey premotor cortex examined with microstimulation. Neurosci Res, 23(3), 269–279. [PubMed: 8545075]

Gundersen HJ (1986). Stereology of arbitrary particles. A review of unbiased number and size estimators and the presentation of some new ones, in memory of William R. Thompson. J Microsc, 143(Pt 1), 3–45. [PubMed: 3761363]

Hao Y, Zhang Q, Controzzi M, Cipriani C, Li Y, Li J, … Zheng X (2014). Distinct neural patterns enable grasp types decoding in monkey dorsal premotor cortex. J Neural Eng, 11(6), 066011. doi: 10.1088/1741-2560/11/6/066011 [PubMed: 25380169]

He SQ, Dum RP, & Strick PL (1993). Topographic organization of corticospinal projections from the frontal lobe: motor areas on the lateral surface of the hemisphere. J Neurosci, 13(3), 952–980. [PubMed: 7680069]

Hendrix CM, Mason CR, & Ebner TJ (2009). Signaling of grasp dimension and grasp force in dorsal premotor cortex and primary motor cortex neurons during reach to grasp in the monkey. J Neurophysiol, 102(1), 132–145. doi:10.1152/jn.00016.2009 [PubMed: 19403752]

Hoff EC (1935). Corticospinal fibers arising in the premotor area of monkey. Distribution of bouton terminations. Archives of Neurology and Psychiatry, 33(687–697).

Hoshi E, & Tanji J (2007). Distinctions between dorsal and ventral premotor areas: anatomical connectivity and functional properties. Curr Opin Neurobiol, 17(2), 234–242. doi:10.1016/j.conb.2007.02.003 [PubMed: 17317152]

Hudson HM, Park MC, Belhaj-Saif A, & Cheney PD (2017). Representation of individual forelimb muscles in primary motor cortex. J Neurophysiol, 118(1), 47–63. doi:10.1152/jn.01070.2015 [PubMed: 28356482]

Isa T, Ohki Y, Seki K, & Alstermark B (2006). Properties of propriospinal neurons in the C3-C4 segments mediating disynaptic pyramidal excitation to forelimb motoneurons in the macaque monkey. J Neurophysiol, 95(6), 3674–3685. doi:10.1152/jn.00103.2005 [PubMed: 16495365]

Jacobsen CF (1934). The influence of motor and premotor lesions upon retention of acquired skilled movements in monkey and chimpanzees. Assoc Res Nerv Ment Dis, 13, 225–247.

Jacobsen CF (1935). Functions of the frontal association areas in primates. Arch Neurol Psychiatry, 33, 558–569.

Jenny AB, & Inukai J (1983). Principles of motor organization of the monkey cervical spinal cord. J Neurosci, 3(3), 567–575. [PubMed: 6827309]

Kantak SS, Stinear JW, Buch ER, & Cohen LG (2012). Rewiring the brain: potential role of the premotor cortex in motor control, learning, and recovery of function following brain injury. Neurorehabil Neural Repair, 26(3), 282–292. doi:10.1177/1545968311420845 [PubMed: 21926382]

Kinoshita M, Matsui R, Kato S, Hasegawa T, Kasahara H, Isa K, … Isa T (2012). Genetic dissection of the circuit for hand dexterity in primates. Nature, 487(7406), 235–238. doi:10.1038/nature11206 [PubMed: 22722837]

Kurata K, & Hoffman DS (1994). Differential effects of muscimol microinjection into dorsal and ventral aspects of the premotor cortex of monkeys. J Neurophysiol, 71(3), 1151–1164. doi:10.1152/jn.1994.71.3.1151 [PubMed: 8201409]

Kuypers HGJM (1960). Central cortical projections to motor and somato-sensory cell groups. An experimental study in the rhesus monkey. Brain, 83, 161–184. [PubMed: 14413010]

Kuypers HGJM (1962). Corticospinal connections: postnatal development in the rhesus monkey. Science, 138(3541), 678–680. [PubMed: 13927687]

Kuypers HGJM (1964). The Descending Pathways to the Spinal Cord, Their Anatomy and Function. Prog Brain Res, 11, 178–202. [PubMed: 14300477]

Kuypers HGJM & Brinkman J (1970). Precentral projections to different parts of the spinal intermediate zone in therhesus monkey. Brain Res, 24(1), 29–48. [PubMed: 4099987]

Kuypers HG (1982). A new look at the organization of the motor system. Prog Brain Res, 57, 381–403. doi:10.1016/S0079-6123(08)64138-2 [PubMed: 6818612]

Kuypers HGJM (1981). Anatomy of the descending pathways In Brooks VB (Ed.), Handboof of Physiology, section 1. The nervous system, vol. II. Motor Control, Pt I (pp. 597–666). Bethesda, MD: American Physiological Society.

Kwan HC, Mackay WA, Murphy JT, & Wong YC (1978a). An intracortical microstimulation study of output organization in precentral cortex of awake primates. J Physiol (Paris), 74(3), 231–233. [PubMed: 102772]

Kwan HC, MacKay WA, Murphy JT, & Wong YC (1978b). Spatial organization of precentral cortex in awake primates. II. Motor outputs. J Neurophysiol, 41(5), 1120–1131. doi:10.1152/jn.1978.41.5.1120 [PubMed: 100584]

Lawrence DG, & Kuypers HGJM (1968). The functional organization of the motor system in the monkey. II. The effects of lesions of the descending brain-stem pathways. Brain, 91(1), 15–36. [PubMed: 4966860]

Lemon RN (2008a). Descending pathways in motor control. Annu Rev Neurosci, 31, 195–218. doi:10.1146/annurev.neuro.31.060407.125547 [PubMed: 18558853]

Lemon RN (2008b). An enduring map of the motor cortex. Exp Physiol, 93(7), 798–802. doi:10.1113/expphysiol.2007.039081 [PubMed: 18562475]

Lemon RN, Landau W, Tutssel D, & Lawrence DG (2012). Lawrence and Kuypers (1968a, b) revisited: copies of the original filmed material from their classic papers in Brain. Brain, 135(Pt 7), 2290–2295. doi:10.1093/brain/aws037 [PubMed: 22374938]

Lyon W, Mehta TI, Pointer KB, Walden D, Elmayan A, Swanson KI, & Kuo JS (2014). Clinton Woolsey: functional brain mapping pioneer. J Neurosurg, 121(4), 983–988. doi: 10.317/014.6.JNS132030 [PubMed: 25105696]

Martino AM, & Strick PL (1987). Corticospinal projections originate from the arcuate premotor area. Brain Res, 404(1–2), 307–312. [PubMed: 3032334]

Matelli M, Luppino G, & Rizzolatti G (1985). Patterns of cytochrome oxidase activity in the frontal agranular cortex of the macaque monkey. Behav Brain Res, 18(2), 125–136. [PubMed: 3006721]

Matsushita M, Ikeda M, & Hosoya Y (1979). The location of spinal neurons with long descending axons (long descending propriospinal tract neurons) in the cat: a study with the horseradish peroxidase technique. J Comp Neurol, 184(1), 63–80. doi:10.1002/cne.901840105 [PubMed: 84003]

McNeal DW, Darling WG, Ge J, Stilwell-Morecraft KS, Solon KM, Hynes SM, … Morecraft RJ (2010). Selective long-term reorganization of the corticospinal projection from the supplementary motor cortex following recovery from lateral motor cortex injury. J Comp Neurol, 518(5), 586–621. doi:10.1002/cne.22218 [PubMed: 20034062]

Mesulam MM (1982). Tracing Neural Connections with Horseradish Peroxidase. New York: John Wiley and Sons.

Molenaar I (1978). The distribution of propriospinal neurons projecting to different motoneuronal cell groups in the cat's brachial cord. Brain Res, 158(1), 203–206. [PubMed: 21348362]

Molenaar I, & Kuypers HG (1978). Cells of origin of propriospinal fibers and of fibers ascending to supraspinal levels. A HRP study in cat and rhesus monkey. Brain Res, 152(3), 429–450. [PubMed: 80246]

Molenaar I, Rustioni A, & Kuypers HG (1974). The location of cells of origin of the fibers in the ventral and the lateral funiculus of the cat's lumbo-sacral cord. Brain Res, 78(2), 239–254. [PubMed: 4854936]

Morecraft RJ, Ge J, Stilwell-Morecraft KS, McNeal DW, Hynes SM, Pizzimenti MA, …Darling WG (2015). Vulnerability of the medial frontal corticospinal projection accompanies combined lateral frontal and parietal cortex injury in rhesus monkey. J Comp Neurol, 523(4), 669–697. doi:10.1002/cne.23703 [PubMed: 25349147]

Morecraft RJ, Ge J, Stilwell-Morecraft KS, McNeal DW, Hynes SM, Pizzimenti MA, … Darling WG (2016). Frontal and frontoparietal injury differentially affect the ipsilateral corticospinal projection from the nonlesioned hemisphere in monkey (Macaca mulatta). J Comp Neurol, 524(2), 380–407. doi:10.1002/cne.23861 [PubMed: 26224429]

Morecraft RJ, Ge J, Stilwell-Morecraft KS, McNeal DW, Pizzimenti MA, & Darling WG (2013). Terminal distribution of the corticospinal projection from the hand/arm region of the primary motor cortex to the cervical enlargement in rhesus monkey. J Comp Neurol, 521(18), 4205–4235. doi:10.1002/cne.23410 [PubMed: 23840034]

Morecraft RJ, Ge J, Stilwell-Morecraft KS, Rotella DL, Pizzimenti MA, & Darling WG (2018). New Corticopontine Connections in the Primate Brain: Contralateral Projections From the Arm/Hand Area of the Precentral Motor Region. Front Neuroanat, 12, 68. doi:10.3389/fnana.2018.00068 [PubMed: 30174591]

Morecraft RJ, Geula C, & Mesulam MM (1992). Cytoarchitecture and neural afferents of orbitofrontal cortex in the brain of the monkey. J Comp Neurol, 323(3), 341–358. doi:10.1002/cne.903230304 [PubMed: 1460107]

Morecraft RJ, McNeal DW, Stilwell-Morecraft KS, Dvanajscak Z, Ge J, & Schneider P (2007). Localization of arm representation in the cerebral peduncle of the non-human primate. J Comp Neurol, 504(2), 149–167. doi:10.1002/cne.21438 [PubMed: 17626268]

Morecraft RJ, McNeal DW, Stilwell-Morecraft KS, Gedney M, Ge J, Schroeder CM, & van Hoesen GW (2007). Amygdala interconnections with the cingulate motor cortex in the rhesus monkey. J Comp Neurol, 500(1), 134–165. doi:10.1002/cne.21165 [PubMed: 17099887]

Morecraft RJ, Stilwell-Morecraft KS, Cipolloni PB, Ge J, McNeal DW, & Pandya DN (2012). Cytoarchitecture and cortical connections of the anterior cingulate and adjacent somatomotor fields in the rhesus monkey. Brain Res Bull, 87(4–5), 457–497. doi:10.1016/j.brainresbull.2011.12.005 [PubMed: 22240273]

Morecraft RJ, Stilwell-Morecraft KS, Ge J, Cipolloni PB, & Pandya DN (2015). Cytoarchitecture and cortical connections of the anterior insula and adjacent frontal motor fields in the rhesus monkey. Brain Res Bull, 119(Pt A), 52–72. doi:10.1016/j.brainresbull.2015.10.004 [PubMed: 26496798]

Morecraft RJ, & Van Hoesen GW (1992). Cingulate input to the primary and supplementary motor cortices in the rhesus monkey: evidence for somatotopy in areas 24c and 23c. J Comp Neurol, 322(4), 471–489. doi:10.1002/cne.903220403 [PubMed: 1383283]

Murray EA, & Coulter JD (1981). Organization of corticospinal neurons in the monkey. J Comp Neurol, 195(2), 339–365. doi:10.1002/cne.901950212 [PubMed: 7251930]

Napper RMA (2018). Total Number Is Important: Using the Disector Method in Design-Based Stereology to Understand the Structure of the Rodent Brain. Front Neuroanat, 12, 16. doi:10.3389/fnana.2018.00016 [PubMed: 29556178]

Nudo RJ, & Masterton RB (1990). Descending pathways to the spinal cord, III: Sites of origin of the corticospinal tract. J Comp Neurol, 296(4), 559–583. doi:10.1002/cne.902960405 [PubMed: 2113540]

Ohbayashi M, Picard N, & Strick PL (2016). Inactivation of the Dorsal Premotor Area Disrupts Internally Generated, But Not Visually Guided, Sequential Movements. J Neurosci, 36(6), 1971–1976. doi:10.1523/JNEUROSCI.2356-15.2016 [PubMed: 26865620]

Olesen MV, Needham EK, & Pakkenberg B (2017). The Optical Fractionator Technique to Estimate Cell Numbers in a Rat Model of Electroconvulsive Therapy. J Vis Exp(125). doi:10.3791/55737

Pandya D, Petrides M, Seltzer B, Cipolloni PB (2015). Cerebral Cortex: Archtecture, Connections and the Dual Origin Concept. New York: Oxford University Press.

Petrides M, & Pandya DN (2009). Distinct parietal and temporal pathways to the homologues of Broca's area in the monkey. PLoS Biol, 7(8), e1000170. doi:10.1371/journal.pbio.1000170 [PubMed: 19668354]

Pizzimenti MA, Darling WG, Rotella DL, McNeal DW, Herrick JL, Ge J, … Morecraft RJ (2007). Measurement of reaching kinematics and prehensile dexterity in nonhuman primates. J Neurophysiol, 98(2), 1015–1029. doi:10.1152/jn.00354.2007 [PubMed: 17553948]

Plow EB, Cunningham DA, Varnerin N, & Machado A (2015). Rethinking stimulation of the brain in stroke rehabilitation: why higher motor areas might be better alternatives for patients with greater impairments. Neuroscientist, 21(3), 225–240. doi:10.1177/1073858414537381 [PubMed: 24951091]

Prabhu G, Shimazu H, Cerri G, Brochier T, Spinks RL, Maier MA, & Lemon RN (2009). Modulation of primary motor cortex outputs from ventral premotor cortex during visually guided grasp in the macaque monkey. J Physiol, 587(Pt 5), 1057–1069. doi:10.1113/jphysiol.2008.165571 [PubMed: 19139043]

Raos V, Umilta MA, Gallese V, & Fogassi L (2004). Functional properties of grasping-related neurons in the dorsal premotor area F2 of the macaque monkey. J Neurophysiol, 92(4), 1990–2002. doi:10.1152/jn.00154.2004 [PubMed: 15163668]

Rathelot JA, & Strick PL (2009). Subdivisions of primary motor cortex based on cortico-motoneuronal cells. Proc Natl Acad Sci U S A, 106(3), 918–923. doi:10.1073/pnas.0808362106 [PubMed: 19139417]

Reed AF (1940). The nuclear masses in the cervical spinal cord of Macaca mulatto. Journal of Comparative Neurology, 72, 187–206.

Rexed B (1954). A cytoarchitectonic atlas of the spinal cord in the cat. J Comp Neurol, 100(2), 297–379. [PubMed: 13163236]

Rozzi S, Calzavara R, Belmalih A, Borra E, Gregoriou GG, Matelli M, & Luppino G (2006). Cortical connections of the inferior parietal cortical convexity of the macaque monkey. Cereb Cortex, 16(10), 1389–1417. doi:10.1093/cercor/bhj076 [PubMed: 16306322]

Rustioni A, Kuypers HG, & Holstege G (1971). Propiospinal projections from the ventral and lateral funiculi to the motoneurons in the lumbosacral cord of the cat. Brain Res, 34(2), 255–275. [PubMed: 5143120]

Schmidlin E, Brochier T, Maier MA, Kirkwood PA, & Lemon RN (2008). Pronounced reduction of digit motor responses evoked from macaque ventral premotor cortex after reversible inactivation of

the primary motor cortex hand area. J Neurosci, 28(22), 5772–5783. doi:10.1523/JNEUROSCI.0944-08.2008 [PubMed: 18509039]

Shimazu H, Maier MA, Cerri G, Kirkwood PA, & Lemon RN (2004). Macaque ventral premotor cortex exerts powerful facilitation of motor cortex outputs to upper limb motoneurons. J Neurosci, 24(5), 1200–1211. doi:10.1523/JNEUROSCI.4731-03.2004 [PubMed: 14762138]

Sprague JM (1948). A study of motor cell localization in the spinal cord of the rhesus monkey. Am J Anat, 82(1), 1–26. [PubMed: 18919561]

Stark E, Asher I, & Abeles M (2007). Encoding of reach and grasp by single neurons in premotor cortex is independent of recording site. J Neurophysiol, 97(5), 3351–3364. doi:10.1152/jn.01328.2006 [PubMed: 17360824]

Sterling P, & Kuypers HG (1968). Anatomical organization of the brachial spinal cord of the cat. 3. The propriospinal connections. Brain Res, 7(3), 419–443. [PubMed: 5639606]

Takahashi K, Best MD, Huh N, Brown KA, Tobaa AA, & Hatsopoulos NG (2017). Encoding of Both Reaching and Grasping Kinematics in Dorsal and Ventral Premotor Cortices. J Neurosci, 37(7), 1733–1746. doi:10.1523/JNEUROSCI.1537-16.2016 [PubMed: 28077725]

Thompson RF (1999). Clinton Nathan Woolsey: November 30, 1904-January 14, 1993. Biogr Mem Natl Acad Sci, 76, 361–374. [PubMed: 11623765]

Toyoshima K, & Sakai H (1982). Exact cortical extent of the origin of the corticospinal tract (CST) and the quantitative contribution to the CST in different cytoarchitectonic areas. A study with horseradish peroxidase in the monkey. J Hirnforsch, 23(3), 257–269. [PubMed: 7130676]

Weinrich M, & Wise SP (1982). The premotor cortex of the monkey. J Neurosci, 2(9), 1329–1345. [PubMed: 7119878]

West MJ (2012). Basic stereology for biologists and neuroscientists. Cold Spring Harbor Laboratory Press: Cold Spring Harbor, New York.

West MJ, Slomianka L, & Gundersen HJ (1991). Unbiased stereological estimation of the total number of neurons in thesubdivisions of the rat hippocampus using the optical fractionator. Anat Rec, 231(4), 482–497. doi:10.1002/ar.1092310411 [PubMed: 1793176]

Woolsey CN, Settlage PH, Meyer DR, Sencer W, Pinto Hamuy T, & Travis AM (1952). Patterns of localization in precentral and "supplementary" motor areas and their relation to the concept of a premotor area. Res Publ Assoc Res Nerv Ment Dis, 30, 238–264. [PubMed: 12983675]

Woolsey CN (1958). Organization of somatic sensory and motor areas of the cerebral cortex In H. F. a. W. Harlow CN (Ed.), Biological and Biochemical Bases of Behavior. (pp. 63–81). Madison, Wisconsin: University of Wisconsin Press.

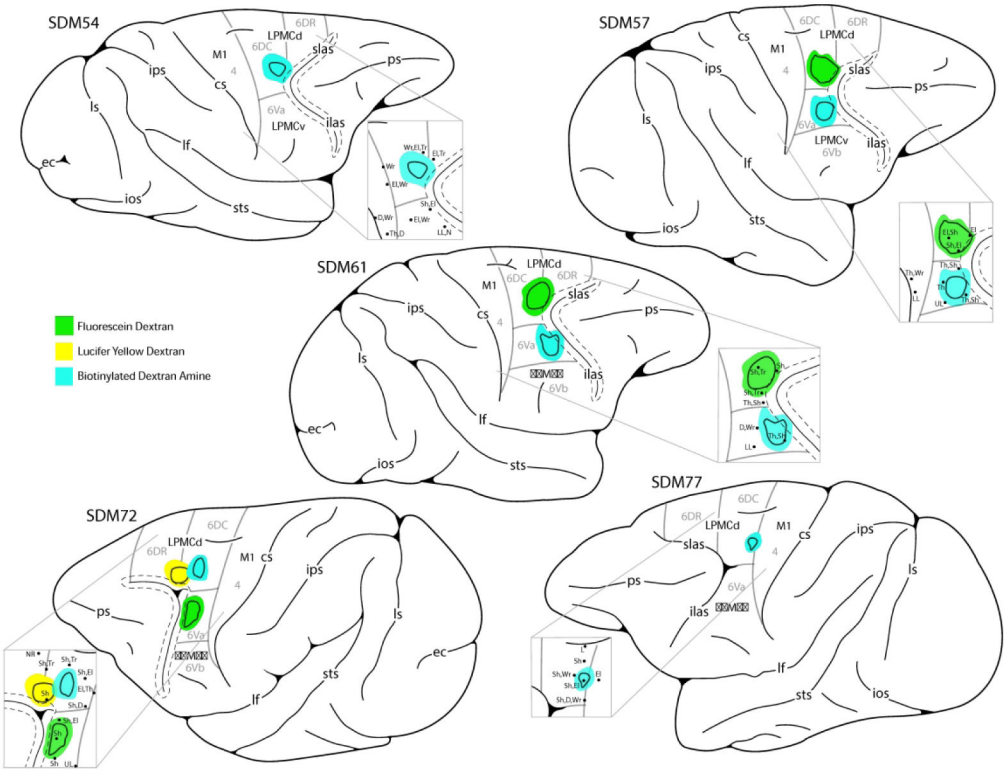

Figure 1.

Line drawings of cortical injection sites located in the dorsal (d) and ventral (v) regions of the lateral premotor cortex (LPMC) of the monkey (*Macaca mulatta*). The arcuate sulcus has been opened which is indicated by the dashed lines around the solid line (the later representing the fundus of the sulcus). Injection sites are color coded for respective dextran tracer and match the legend in the bottom center of the diagram. The solid line within each injection site marks the estimated boundary between the injection site core (in center) and halo which is external to the core region. Cytoarchitectonic borders of the lateral premotor region (areas 4, 6DC, 6DR, 6Va and 6Vb, according to Morecraft et al., 2012, 2015 and Pandya et al., 2015) are marked by the light gray lines. Abbreviations : cs, central sulcus; ec, ectocalcarine sulcus; D, digit; El, elbow; ilas, inferior limb of the arcuate sulcus; ios, inferior occipital sulcus; ips, intraparietal sulcus; L, leg; LL, lower lip; LPMCd, dorsal lateral premotor cortex; LPMCv, ventral lateral premotor cortex; lf, lateral fissure; ls, lunate sulcus; M1, primary motor cortex; N, neck; NR, no response; ps, principle sulcus; SDM, South Dakota Monkey; Sh, shoulder; slas, superior limb of the arcuate sulcus; sts, superior temporal sulcus; Th, thumb; Tr, trunk; UL, upper lip; Wr, wrist.

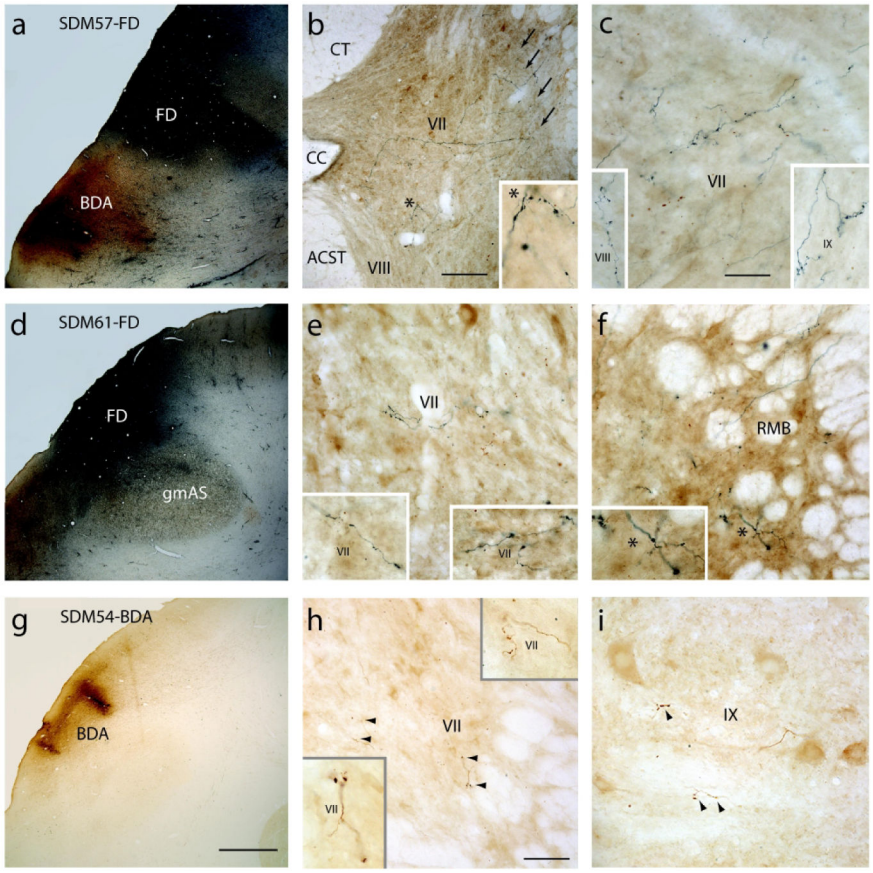

Figure 2.

Plate of photomicrographs showing the major LPMCd injection site cases and representative terminal labeling at C5 to T1 in the spinal cord. A) Coronal section in case SDM57 showing the FD (blue reaction product) and BDA (brown reaction product) injection sites in LPMCd and LPMCv respectively. B) Transverse section in case SDM57-FD showing contralateral FD labeled fibers and terminals in C6. The asterisk in the main panel denotes the location of the higher power image shown in the inset on the bottom right. The arrows (top right) show the main route and trajectory taken by labeled axons from the lateral corticospinal tract to the contralateral spinal gray matter. Note the heavy presence of both axons in passage and labeled bouton terminals in the dorsolateral gray matter region (of lamina VII) that precluded the positive assessment of terminal labeling by Kuypers with his use of the axon degeneration technique that was available at the time he conducted his classical studies. C) Transverse section in case SDM57-FD showing contralateral FD labeled fibers and terminals in the ventromedial sector of lamina VII at C6. The inset on the bottom left shows contralateral terminal labeling in lamina VIII at C5. The inset on the bottom right shows contralateral terminal labeling in lamina IX at C7. D) Low power image showing the FD injection site in case SDM61 just superior to the gray matter capping the posterior tip of the spur of the arcuate sulcus (gmAS). E) Transverse spinal cord section in case SDM61-FD showing terminal labeling in the contralateral ventromedial sector of lamina VII at C5. The inset on the bottom left and bottom right show higher power images of terminal labeling in the ventromedial region of lamina VII at C6 and C7 respectively. F) Transverse section in

case SDM61-FD showing contralateral FD labeled fibers and terminals in the reticulated marginal border (RMB) at C7. The asterisk in the main panel denotes the location of the higher power image shown in the inset on the bottom left. G) Coronal section in case SDM54 showing a portion of the BDA injection site in LPMCd. H) Transverse section through spinal level C6 in case SDM54-BDA showing contralateral terminal labeling in the ventrolateral sector of lamina VII at C6. The arrowheads denote the locations of labeled boutons. The insets are higher power images of BDA lamina VII labeling at C6 (bottom left) and C7 (top right). I) Contralateral terminal labeling in lamina IX in case SDM54-BDA at C5. The arrowheads show locations of terminal bouton profiles. Micron bar in: B = 200μm; C = 50μm and applies to panels E, F and I; G = 2mm and applies to panels A and D; H = 100μm. Abbreviations: ACST, anterior corticospinal tract; CC, central canal; CT, cuneate tract; RMB, reticulated marginal border.

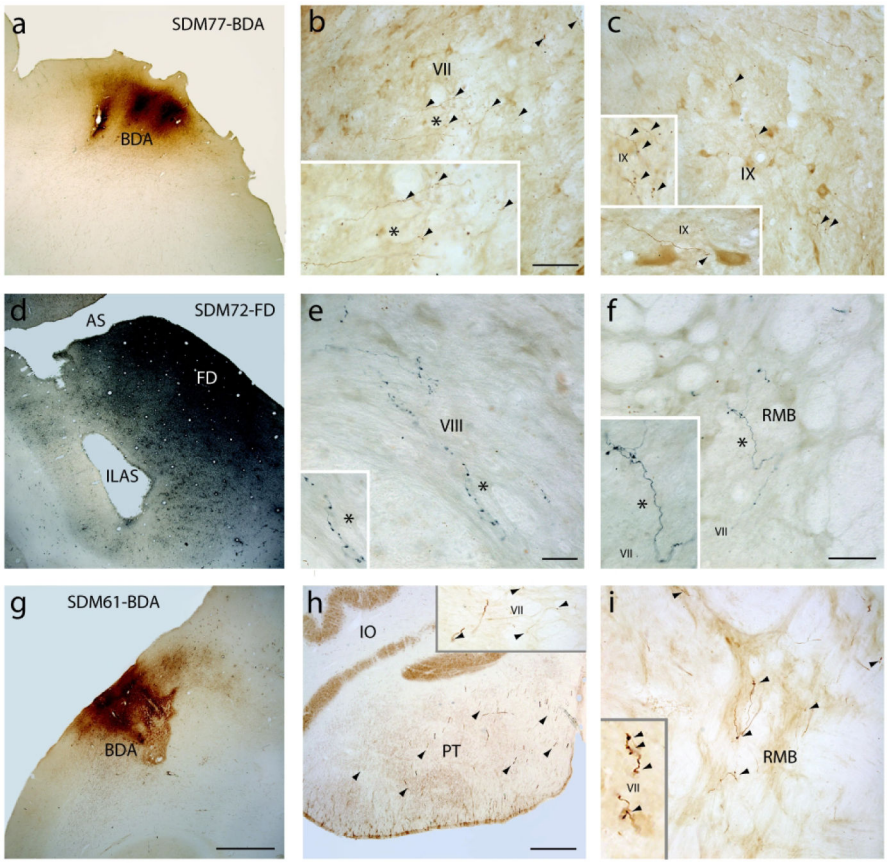

Figure 3.

Photomicrographs showing the injection site in the M1-LPMCd transition area (SDM72-FD) and injection sites in LPMCv (SDM72-FD, SDM61-BDA) and representative terminal labeling in the spinal cord. A) Coronal section in case SDM77-BDA showing the BDA (brown reaction product) injection site that was located in the transition region between M1 (area 4) and LPMCd (area 6DC). The sulcus above the injection site is the superior precentral sulcus. B) Transverse section in case SDM77-BDA showing contralateral BDA labeled fibers and terminals (arrowheads) in the dorsolateral sector of lamina VII at C6. The asterisk in the main panel denotes the location of the higher power image shown in the inset on the bottom left. C) Contralateral terminal labeling in lamina IX in case SDM77-BDA at C7. The insets located on the left of the panel are higher power images showing BDA terminals in lamina IX at C7 (top) and C8 (bottom). The arrowheads show locations of terminal bouton profiles. D) Low power image showing the injection site in case SDM72-FD in the post-arcuate region of LPMCv just below the spur of the arcuate sulcus (AS). E) Transverse section in case SDM72-FD showing contralateral FD labeled fibers and terminals in lamina VIII at C6. The asterisk in the main panel denotes the location of the higher power image shown in the inset on the bottom left. F) Transverse section in case SDM72-FD showing contralateral FD labeled fibers and terminals in the reticulated marginal border (RMB) at C7. The asterisk in the main panel denotes the location of the higher power image shown in the inset on the bottom left. G) Coronal section in case SDM61 showing a portion of the BDA injection site in LPMCv located on the lateral convexity. H) Terminal labeling in

the pyramidal tract at the lower level of the medulla in case SDM61-BDA demonstrating excellent and abundant BDA tracer transport in this experiment (arrowheads identify some clustered labeled axons. The inset on the top right shows a spinal transverse section through C2 with well-filled BDA labeled axons and BDA labeled terminal boutons (arrowheads) in lamina VII in case SDM61-BDA. I) Transverse spinal section in case SDM57-BDA, in which the injection site involved the convexity of LPMCv, showing contralateral BDA labeled fibers and terminal boutons (arrowheads) in the RMB at C1. The inset on the bottom left shows a higher power image of labeled boutons (arrowheads) in lamina VII at C2. Micron bar in: B = 100μm and applies to C and I; E = 25μm; F = 50μm; G = 2mm and applies to A and D; H = 500 μm. Abbreviations: ILAS, inferior limb of the arcuate sulcus; IO, inferior olive; RMB, reticulated marginal border.

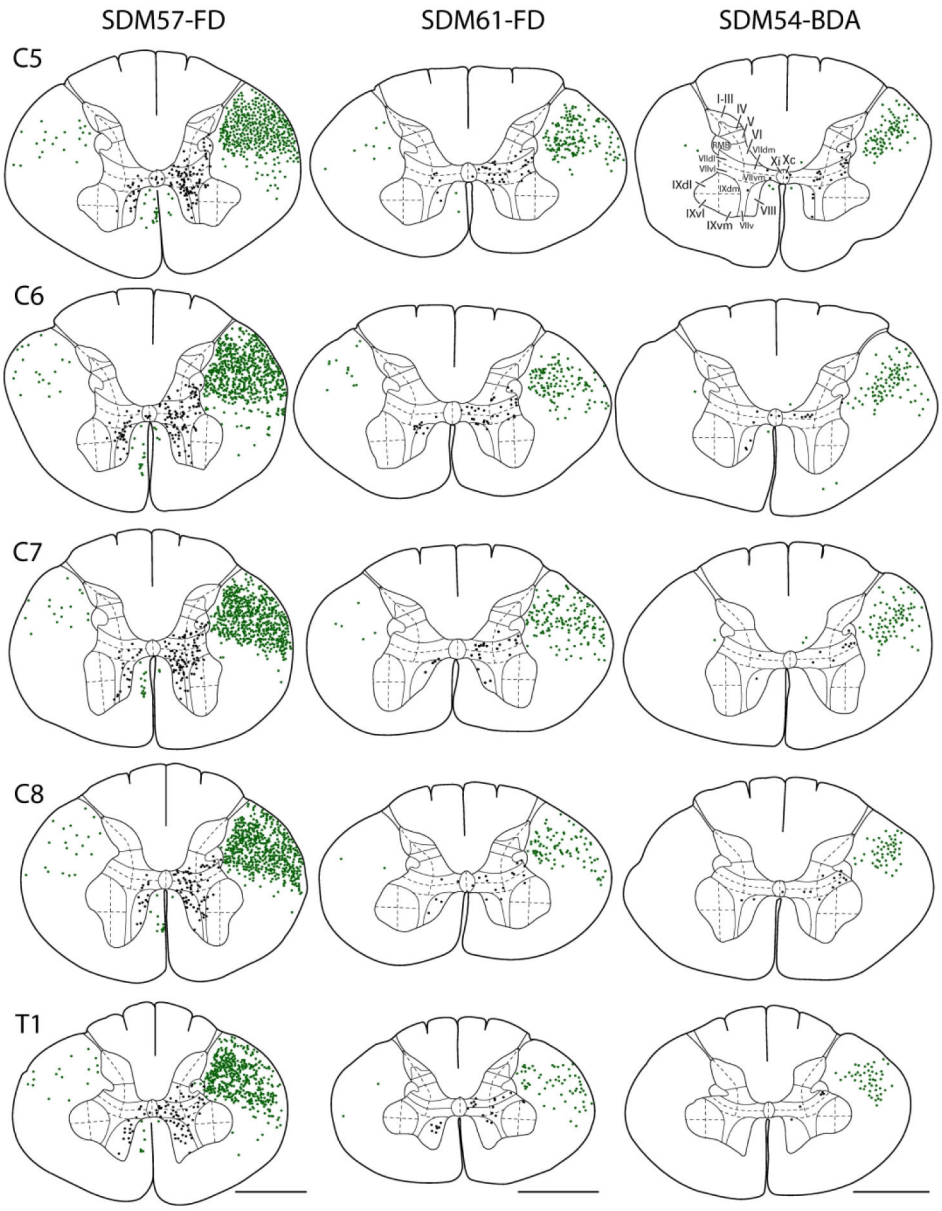

Figure 4.

Line drawings of representative transverse sections through spinal levels C5-T1 from the 3 main LPMCd cases (SDM57-FD, SDM61-FD and SDM54-BDA) depicting the locations of labeled white matter axons (green dots) and locations of labeled gray matter axon terminals (black dots). Spinal levels are depicted on the left (C5, top –T1, bottom) and correspond to all cases. Roman numerals in section C5 of case SDM54-BDA denote Rexed's laminae and their respective anatomical subsectors used for quantitative stereological analysis of terminal bouton numbers. For orientation, dorsal is located on the top of each section and ventral at the bottom. Note the particularly dense distribution of spinal terminals in case SDM57-FD compared to the lighter terminal pattern found in cases SDM61-FD and SDM54-BDA. Abbreviations: dm, dorsomedial; dl, dorsolateral; v, ventral; vl, ventrolateral; vm, ventromedial. Scale bar = 2mm.

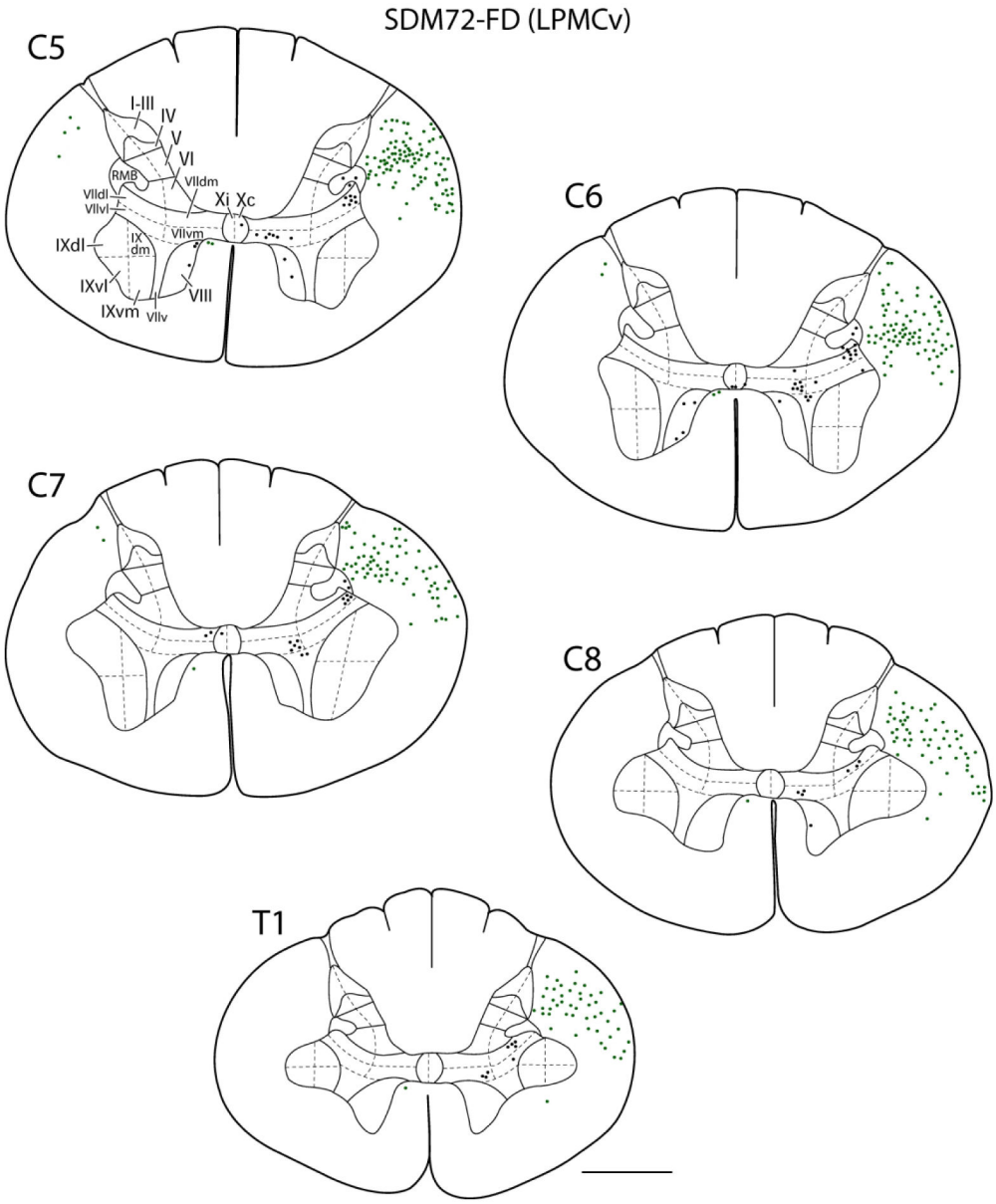

Figure 5.

Line drawings of representative transverse sections through spinal levels C5-T1 from LPMCv case SDM72-FD depicting the locations labeled white matter axons (green dots) and locations of labeled gray matter axon terminals (black dots). Spinal levels are depicted on the top left of each transverse section. Roman numerals in section C5 denote Rexed's laminae and their respective anatomical subsectors used for quantitative stereological analysis of terminal bouton numbers. For orientation dorsal is located on the top of each section and ventral at the bottom. Note the significantly lighter distribution of spinal terminals compared to the LPMCd cases shown in Figure 4. Abbreviations, dm, dorsomedial; dl, dorsolateral; v, ventral; vl, ventrolateral; vm, ventromedial. Scale bar = 2mm.

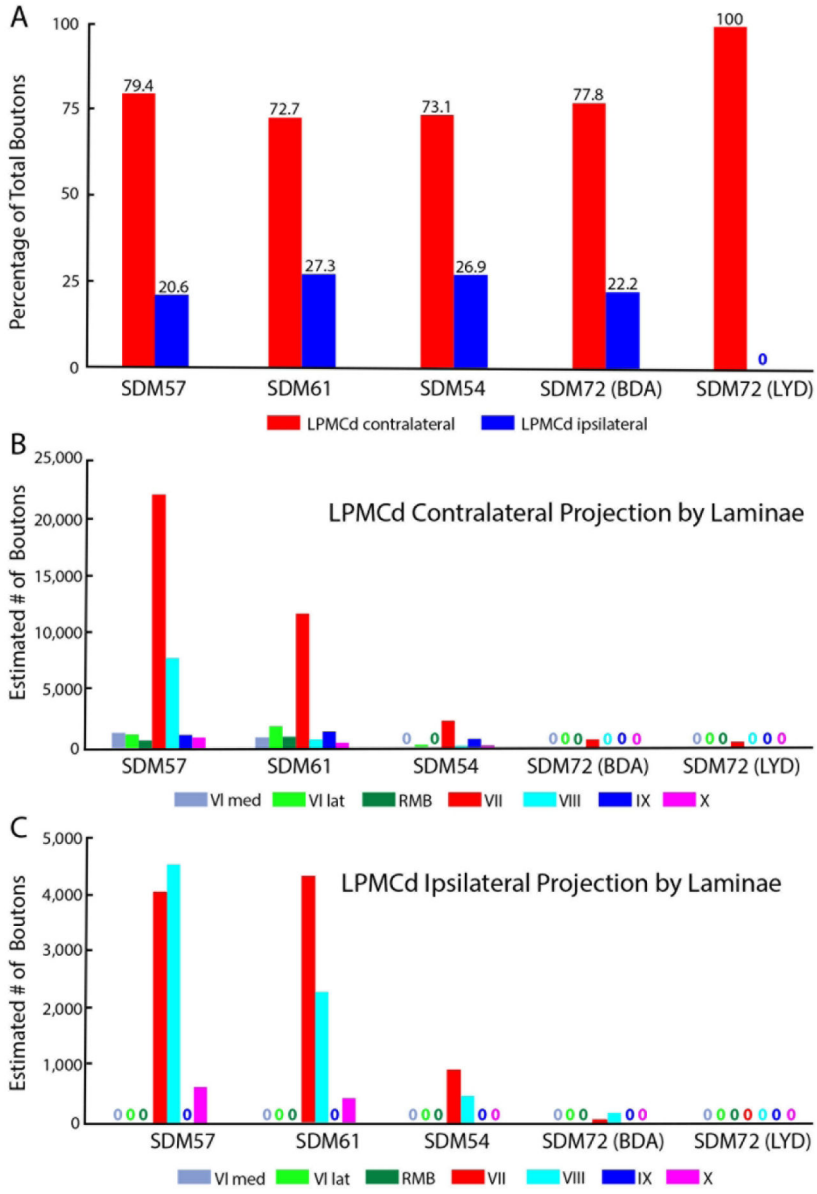

Figure 6.

Percent of total estimated labeled boutons (A) distributed in the contralateral (red bars) and ipsilateral (blue bars) spinal laminae in spinal segments C5-T1 from each LPMCd case. Each bar is the percentage of boutons from each individual LPMCd case with the actual percentage given directly above the bar. Estimated number of contralateral (B) and ipsilateral (C) boutons in Rexed's laminae at C5-T1 in each LPMCd case. Each bar represents the stereological estimate of total number of labeled boutons in Rexed's laminae (denoted by Roman numerals) and the reticulated marginal border (RMB). No labeling within a given Rexed's lamina is denoted with an appropriately color coded "zero" in this figure and all other graph figures. Note that lamina VI is divided into medial and lateral subsectors. In this study, lamina VII was subdivided into 5 subsectors and lamina IX into 4

quadrants and the data for bouton number within these subsectors is shown in subsequent figures. Note the different ordinate scales in B and C

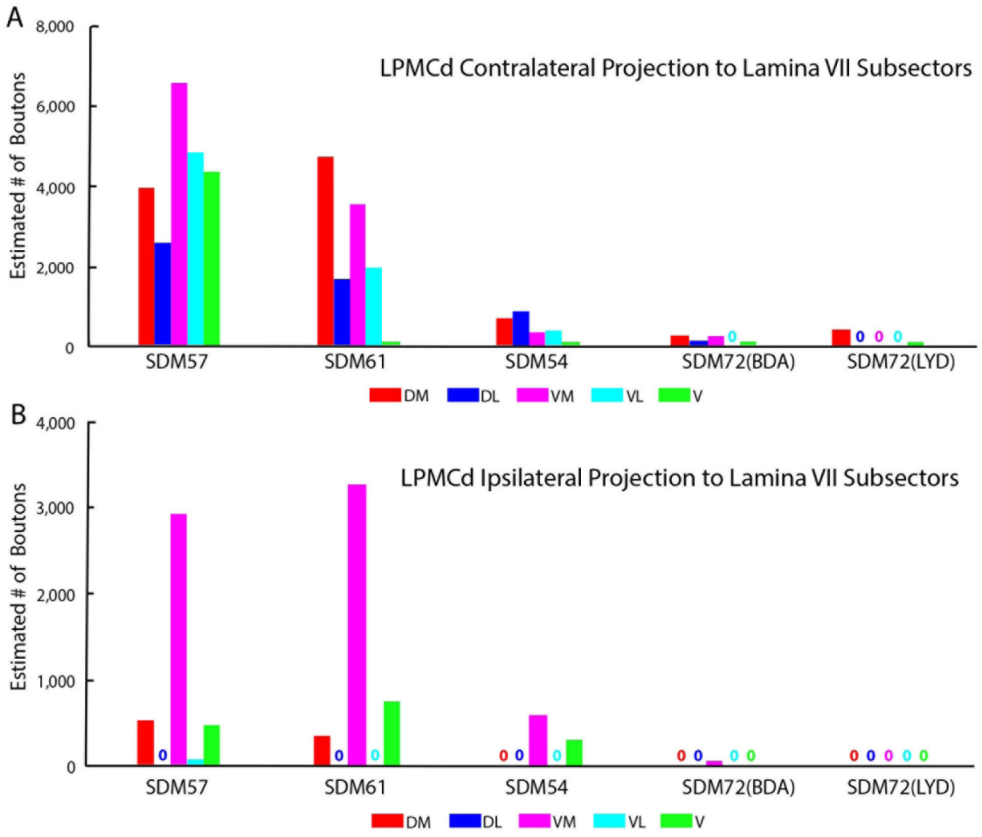

Figure 7.

Estimated number of boutons of the contralateral (A) and ipsilateral (B) corticospinal projection from LPMCd to the anatomical subsectors of lamina VII of spinal segments C5-T1 in all LPMCd injection site cases. Each bar is the estimated number of boutons in each specified lamina VII subsector for an individual case as indicated on the abscissa. Note the general and gradual decline in total bouton numbers from cases SDM57-FD, in which the injection site was located most caudally in LPMCd, to case SDM72-LYD where the injection site was located most rostrally in LPMCd. Subsector abbreviations: DM, dorsomedial; DL, dorsolateral; VM, ventromedial; VL, ventrolateral; V, ventral

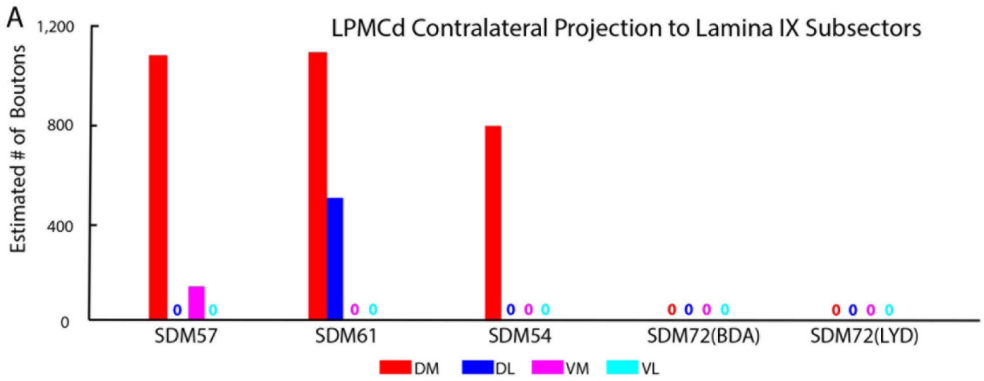

Figure 8.

Estimated number of labeled boutons of the contralateral corticospinal projection to the anatomical subsectors of lamina IX in all LPMCd injection site cases. Each bar is the estimated number of boutons in each specified lamina IX subsector for an individual case as indicated on the abscissa. Note the consistent and prominent distribution of terminal LPMCd labeling in the dorsomedial quadrant in major LPMCd cases SDM57-FD, SDM61-FD and SDM54-BDA. Subsector abbreviations: DM, dorsomedial, DL; dorsolateral; VM, ventromedial; VL, ventrolateral.

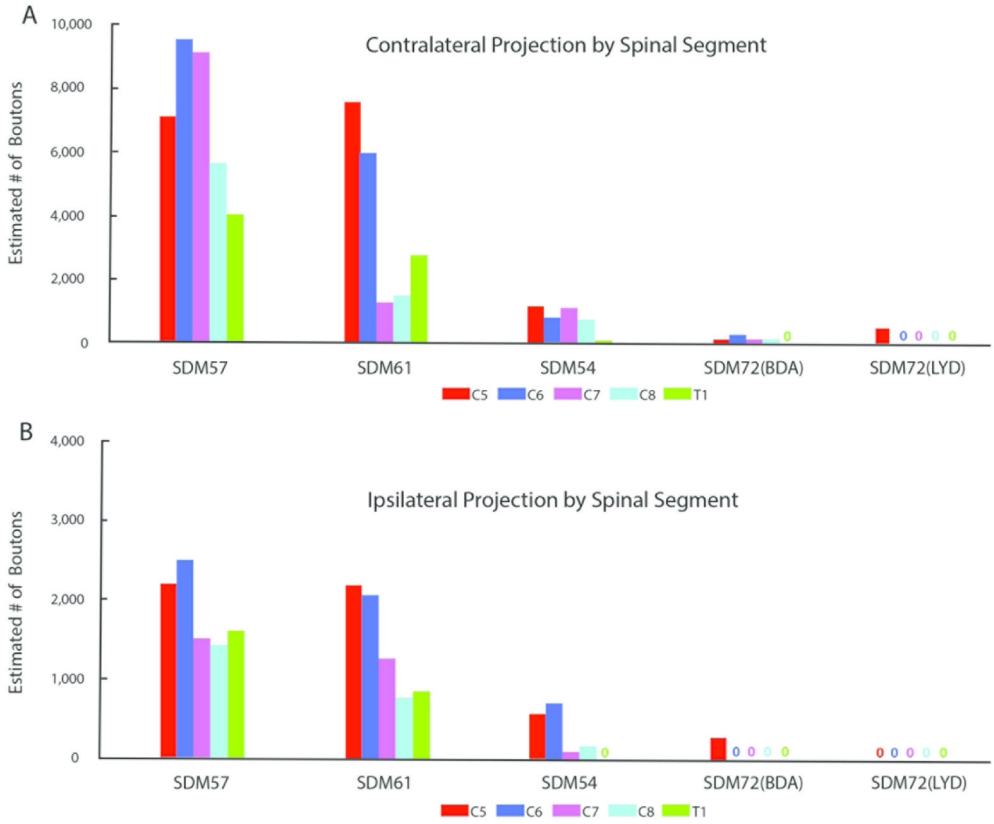

Figure 9.

Estimated number of contralateral (A) and ipsilateral (B) labeled boutons to each spinal segment of C5-T1 in each Figure 9. LPMCd injection site case. Each bar represents the stereological estimate of the total number of boutons in one spinal segment of a single case

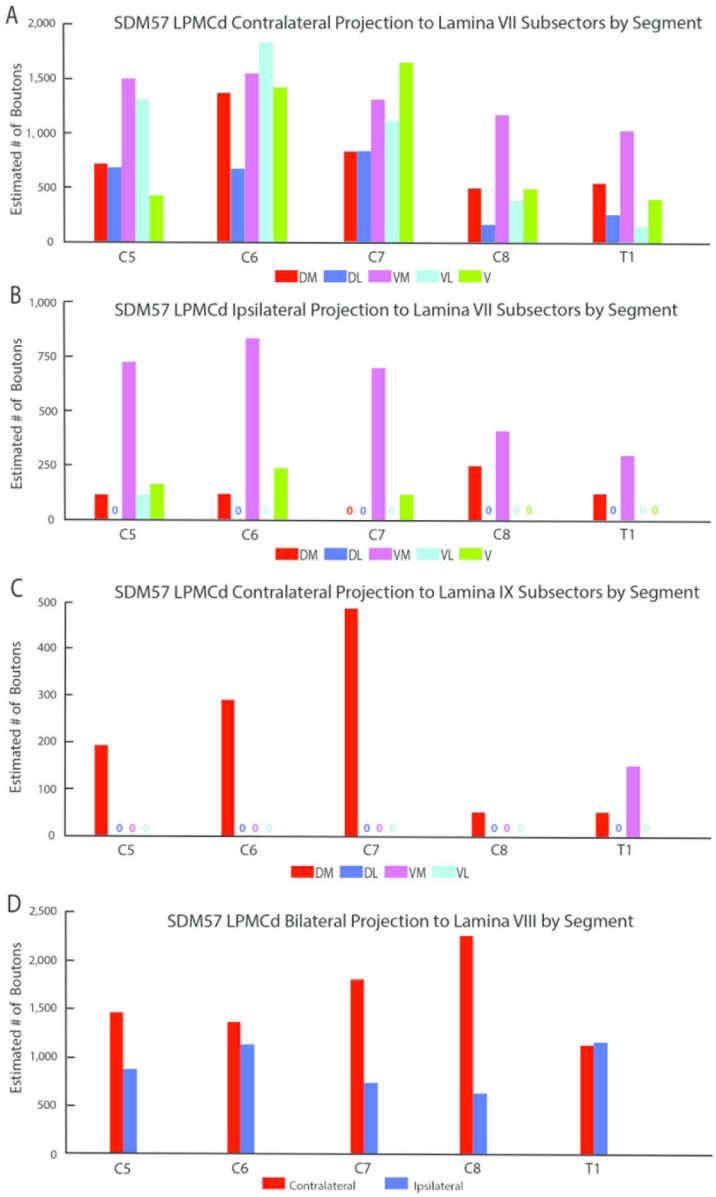

Figure 10.

Estimated number of boutons of the contralateral (A) and ipsilateral (B) corticospinal projection from LPMCd case SDM57-FD to the anatomical subsectors of lamina VII of each spinal segment (C5-T1). Each bar is the estimated number of boutons in each specified lamina VII subsector. Estimated number of boutons of the contralateral corticospinal projection (C) from LPMCd case SDM57-FD to the anatomical subsectors of lamina IX at each spinal segment (C5-T1). As indicated the greatest number of labeled boutons occurred at levels C5-C7. Each bar is the estimated number of boutons in each specified lamina IX subsector. Estimated number of labeled boutons of the bilateral CSP (D) from case SDM57-FD to lamina VIII at each spinal segment (C5-T1). Note the stepwise increase of contralateral lamina VIII labeling from C5-C8 and strong bilateral terminal labeling at T1, which was relatively equivalent to the amount of terminal lamina VIII labeling found at C5

and C6. Subsector abbreviations: DM, dorsomedial; DL, dorsolateral; VM, ventromedial; VL, ventrolateral; V, ventral

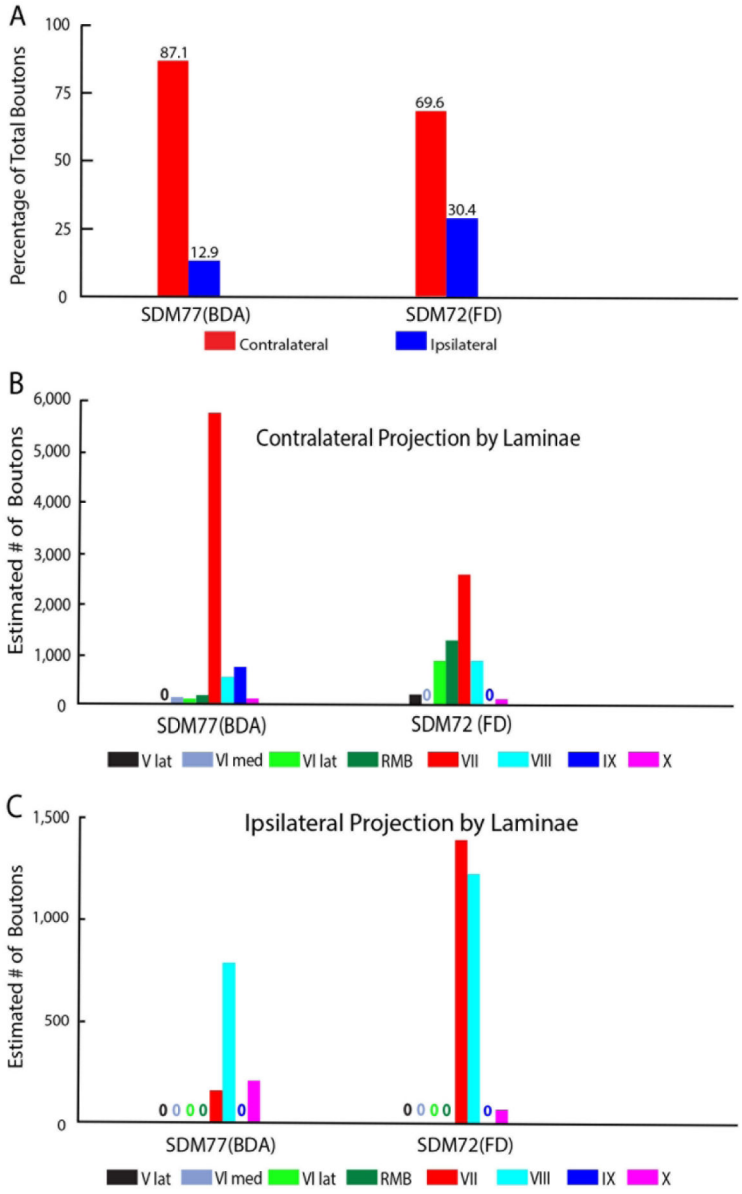

Figure 11.

Percent of total estimated labeled boutons (A) distributed in the contralateral (red bars) and ipsilateral (blue bars) spinal laminae in segments C5-T1 following dextran tracer injection in experimental case SDM77-BDA (which involved the M1/LPMCd transition area) and case SDM72-FD (which involved the post-arcuate region of LPMCv). Each bar is the percentage of boutons from each individual case with the actual percentage given directly above the bar. Estimated number of contralateral (B) and ipsilateral (C) boutons in Rexed's laminae at C5-T1 in each case. Each bar represents the stereological estimate of total number of labeled boutons in Rexeds' laminae (denoted by Roman numerals) and the reticulated marginal border (RMB)

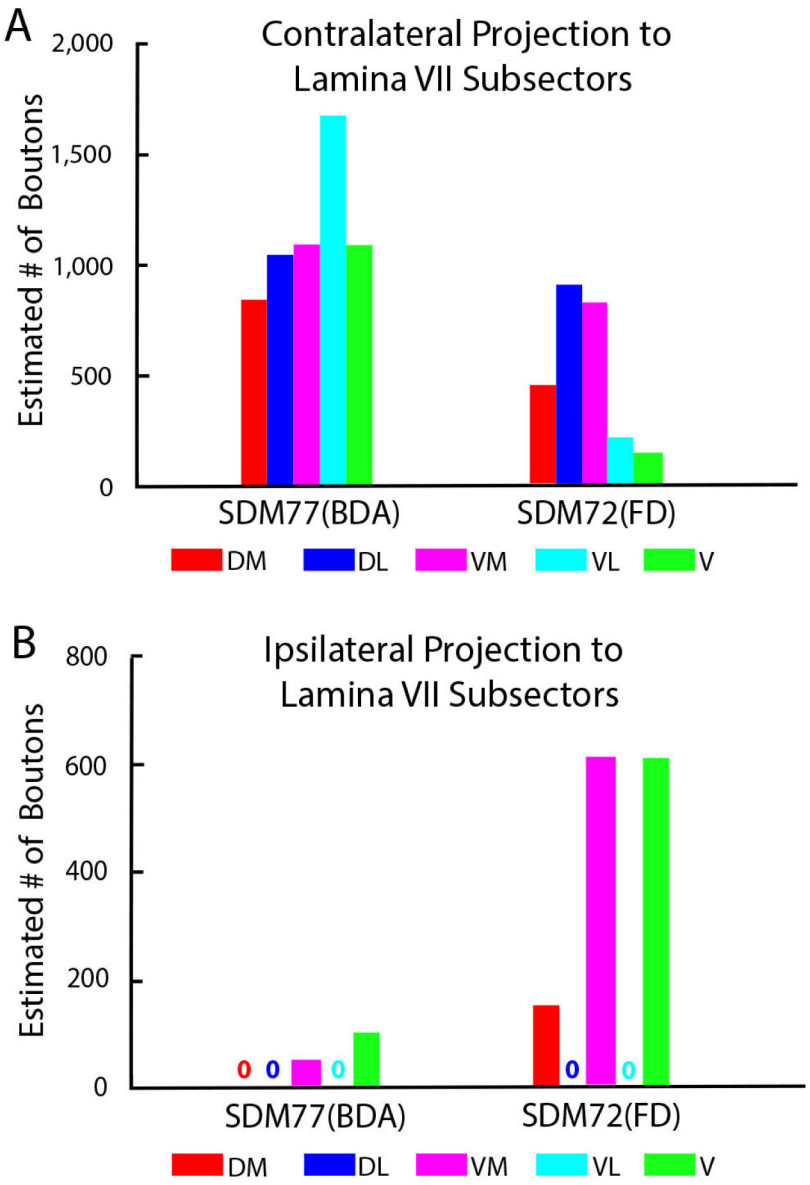

Figure 12.

Estimated number of boutons of the contralateral (A) and ipsilateral (B) corticospinal projection from injection site SDM77-BDA (M1/LPMCd transition area) and case SDM72-FD (LPMCv post-arcuate area) within the anatomical subsectors of lamina VII of spinal segments C5-T1. Each Bar is the estimated number of boutons in each specified lamina VII subsector for an individual case as indicated on the abscissa. Subsector abbreviations: DM, dorsomedial; DL, dorsolateral; VM, ventromedial; VL, ventrolateral; V, ventral

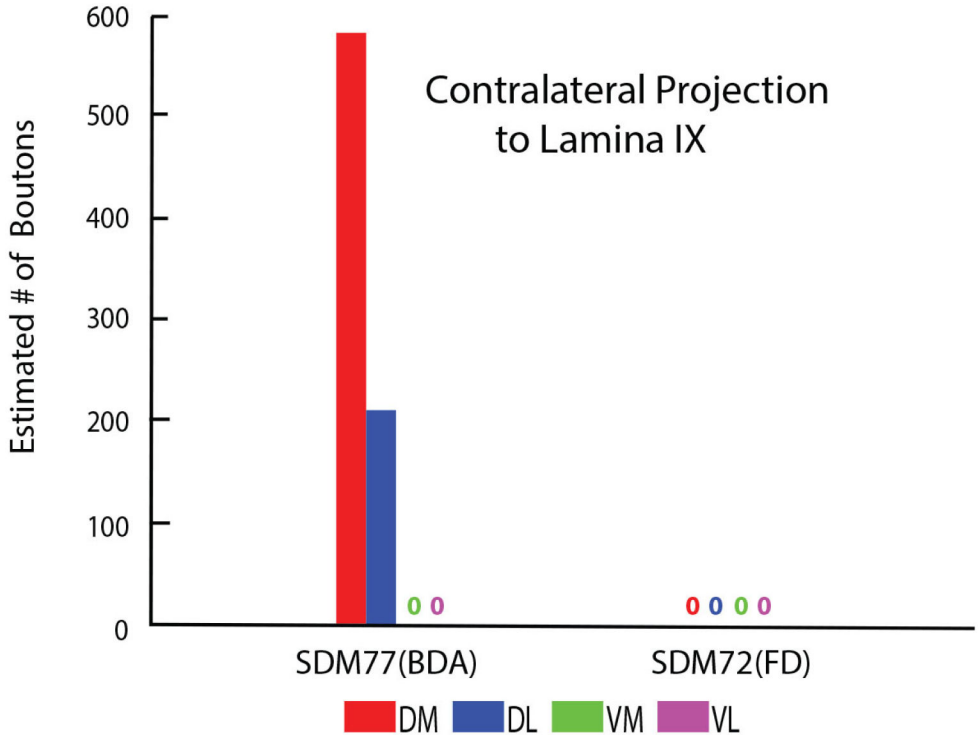

Figure 13.

Estimated number of labeled boutons of the contralateral corticospinal projection to the anatomical subsectors of lamina IX in injection site case SDM77-BDA (M1/LPMCd transition area) and injection site case SDM72-FD (LPMCv post-arcuate area). Each bar is the estimated number of boutons in each specified lamina VII subsector for an individual case as indicated on the abscissa. Note the prominent distribution of terminal LPMCd/M1 labeling in the dorsomedial and dorsolateral quadrants in case SDM77-BDA. In contrast, no labeling was found in lamina IX in case SDM72-FD. Subsector abbreviations: DM, dorsomedial; DL, dorsolateral; VM, ventromedial; VL, ventrolateral.

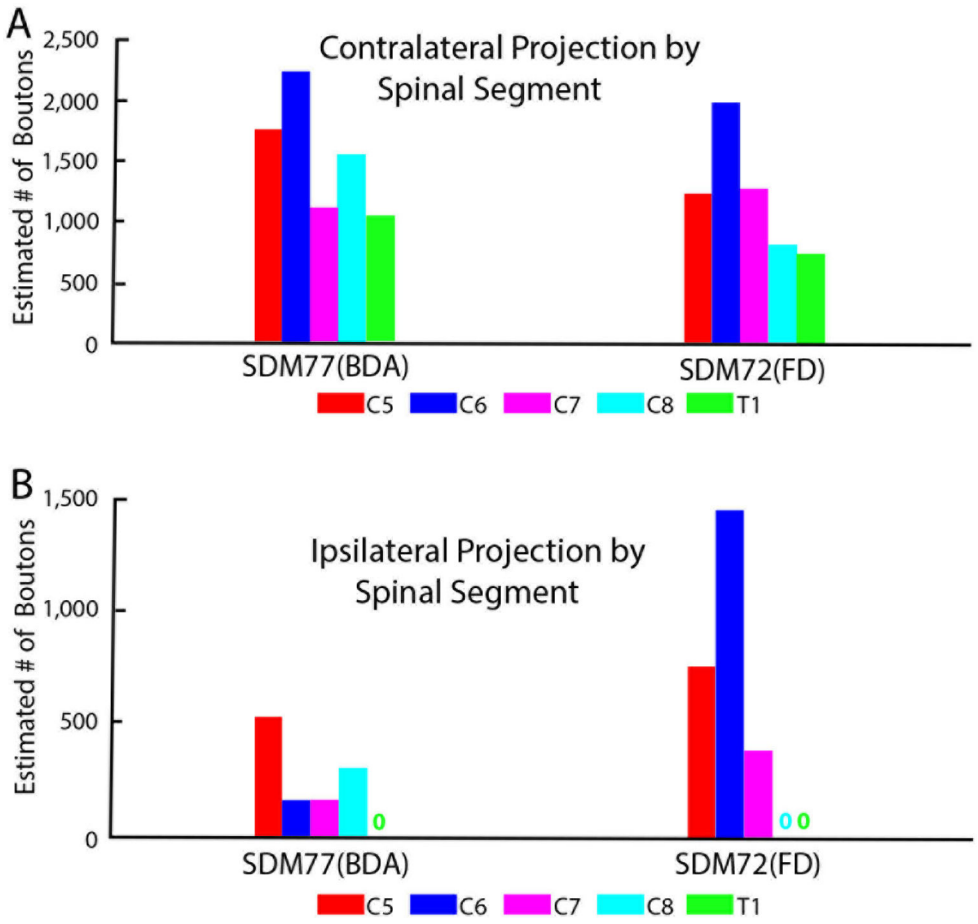

Figure 14.

Estimated number of contralateral (A) and ipsilateral (B) labeled boutons within spinal segments C5-T1 in case SDM77-BDA (M1/LPMCd transition area) and case SDM72-FD (LPMCv post-arcuate area). Each bar represents the stereological estimate of the total number of boutons in one spinal segment of a single case.

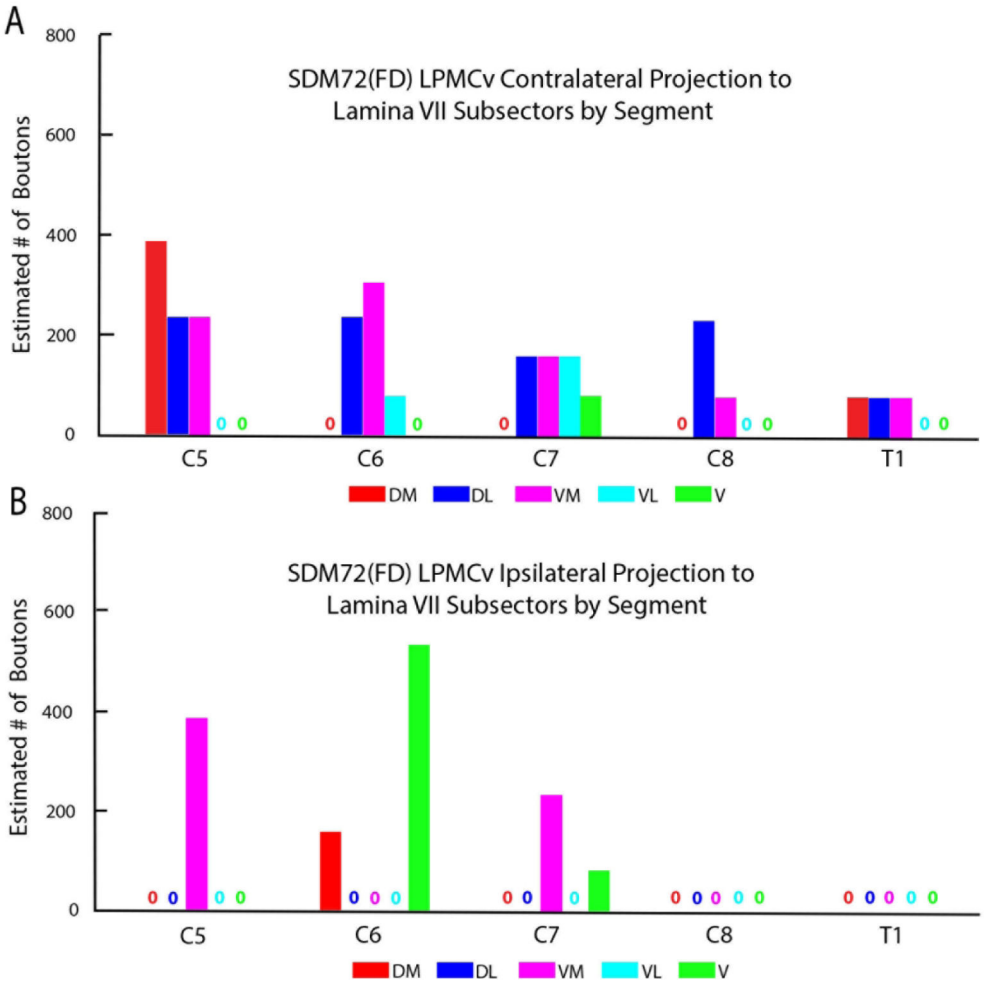

Figure 15.

Estimated number of boutons of the contralateral (A) and ipsilateral (B) corticospinal projection from post-arcuate LPMCv case SDM72-FD to the anatomical subsectors of lamina VII of spinal segments C5-T1. Each bar is the estimated number of boutons in each specified lamina VII subsector of a single spinal segment. Subsector abbreviations: DM, dorsomedial; DL, dorsolateral; VM, ventromedial; VL, ventrolateral; V, ventral

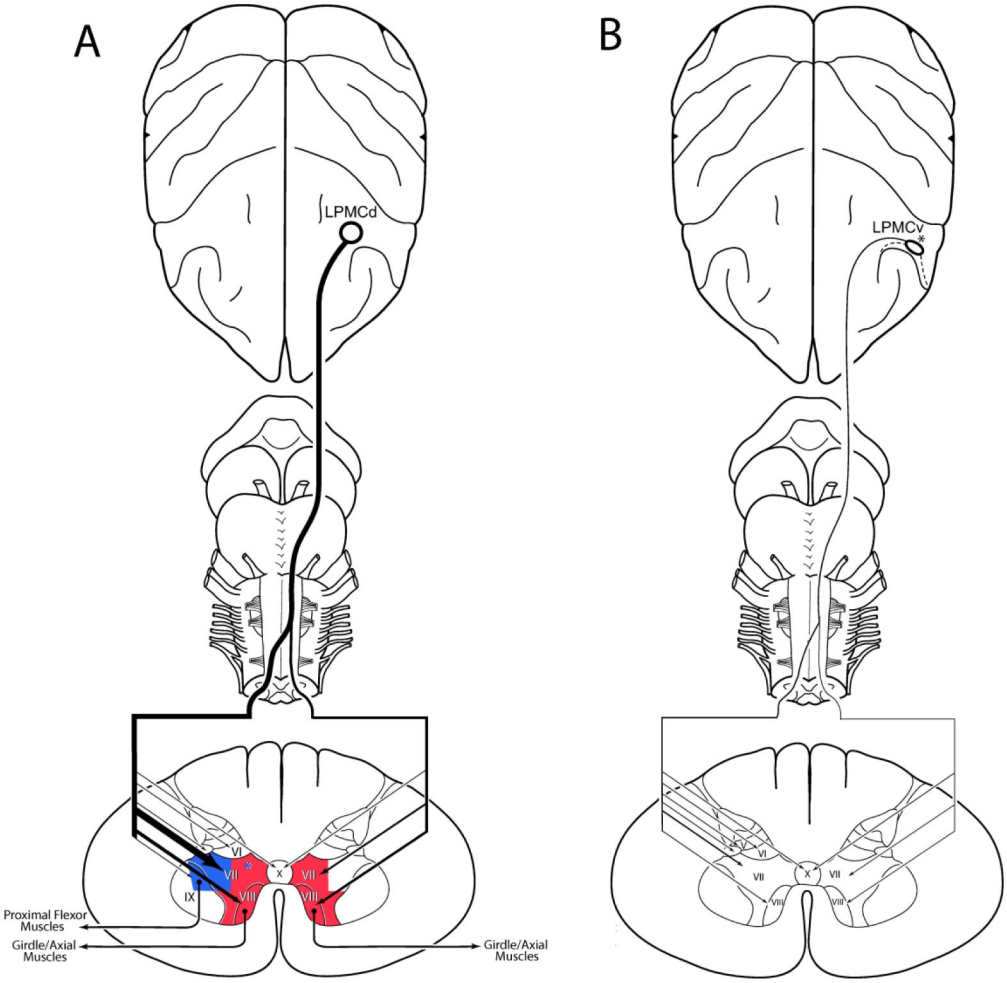

Figure 16.

Summary diagrams of the main findings of the study. The left diagram (A) illustrates in schematic fashion the overall LPMCd corticospinal projection to the cervical enlargement from case SDM57-FD, which gave rise to the most prominent CSP of all LPMCd experimental cases. The relative intensity of the projection to spinal cord laminae is indicated by line thickness and arrowhead size. Strong bilateral projections were found to the medial and ventral parts of lamina VII and lamina VIII which are considered major targets of Kuypers medial motor system (shaded in red) which largely influences proximal limb and axial movements. In addition, a strong projection was found to the lateral sectors of contralateral lamina VII which are considered major components of Kuypers “lateral motor system” (shaded in blue) which largely influences distal limb movements. The blue asterisk located within the dorsomedial region of lamina VII denotes an area of CSP terminal overlap amongst the M1 hand CSP of the lateral motor system, and LPMCd CSP of the medial motor system. The right diagram (B) illustrates the overall LPMCv corticospinal projection to the cervical enlargement from case SDM72-FD, which originated from the post-arcuate cortical region. As indicated by the thin lines representing the relative projections to Rexed’s laminae, this CSP was sparse compared to the more prominent LPMCd CSP shown on the left. The white area located in anterior to the dashed line on the cortical surface represents

the cortex lining the posterior bank of the arcuate sulcus. The black asterisk on the cortical surface that is posterior to the post-arcuate region denotes cortex located on the convexity that did not project below C2.

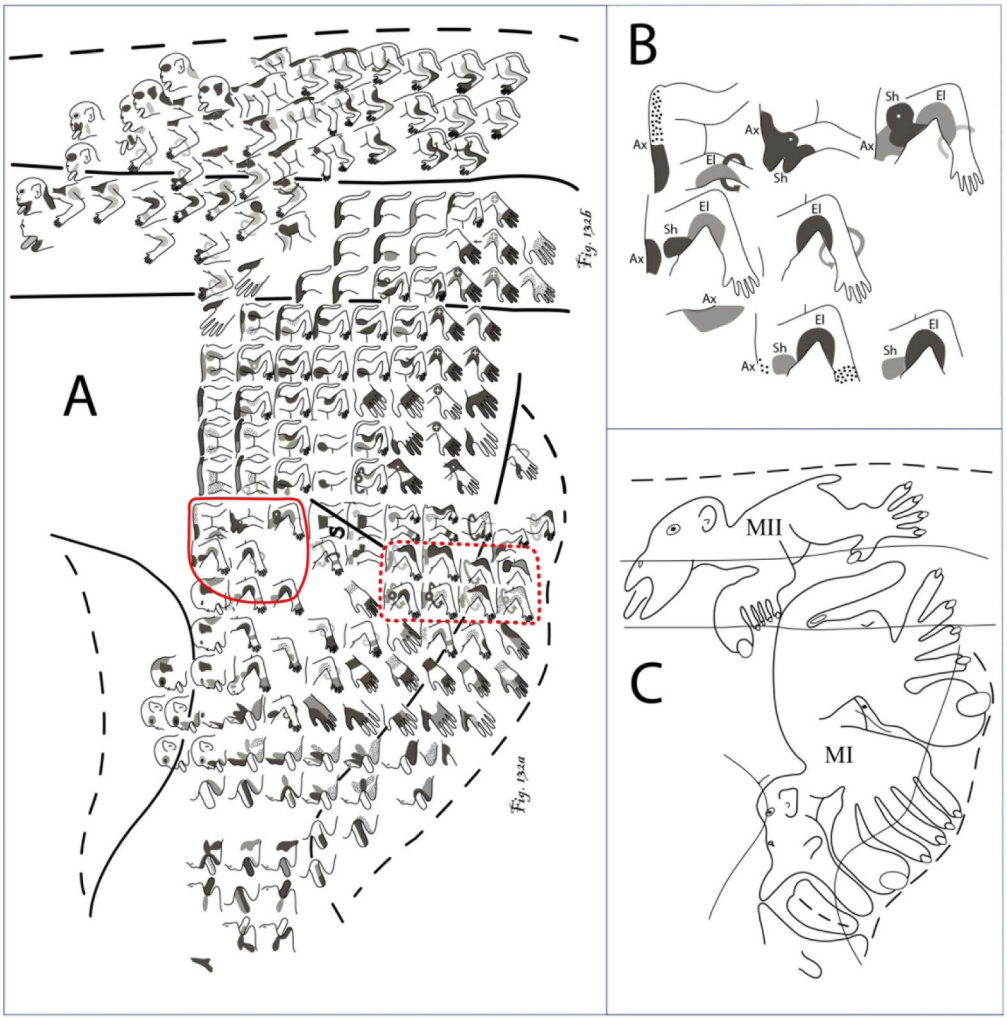

Figure 17.

Modified reproduction of Woolsey's composite figurine map of precentral and supplementary motor area movement representation from his epicortical stimulation observations in 22 monkey cases (Woolsey et al., 1952). Within each figurine, solid black signifies the strongest and earliest evoked movements, gray shading represents intermediate effects, and stippling denotes the weakest effects. Although simplified, Woolsey emphasizes in numerous locations of his manuscript that extensive overlap occurs in the cortical motor patterns and there are no sharp lines of demarcation, and he keenly points out that "… the figurine method of illustration, although it is not ideal, may help the reader not only to visualize the foci for movement of different parts of the body but also to see the extent to which adjacent centers mutually overlap". The area outlined by the solid red line represents the cortical location corresponding to our injection site in LPMCd case SDM57-FD. The area outlined by the dotted red line denotes the precentral location of the M1 shoulder representation, which is positioned between the M1 hand and M1 leg representations. B) Enlargement of the area outlined by the solid red line in panel A. Note the extensive representation of axial, shoulder and elbow movements. C) Woolsey's summary diagram showing the basic spatial relationship between the precentral motor area (M1) and

supplementary motor area (MII). Abbreviations: Ax, axial movement; El, elbow movement, Sh, shoulder movement.

Table 1.

Description of the Experimental Parameters in each Case

Case	Sex	Age (yrs.)	Weight (kg)	Area Injected	Tracer/ Injections	Total Volume (μL	Injection Core Vol. (mm^3)	Injection Halo Vol. (mm^3)	Post-injection Survival (days)
SDM54	Male	9.0	9.2	LPMCd	BDA/3	1.2	15.44	78.44	33
SDM57	Female	18.0	6.0	LPMCd	FD/3	1.2	15.33	78.44	32
				LPMCv	BDA/3	1.2	4.01	21.43	
SDM61	Female	4.0	4.3	LPMCd	FD/3	1.2	20.82	96.55	33
				LPMCv	BDA/3	1.2	5.47	28.07	
SDM72	Female	8.7	5.6	LPMCv	FD/3	1.2	7.16	90.32	33
				LPMCd	BDA/3	1.2	3.56	25.06	
				LPMCd	LYD/3	1.2	7.88	52.42	
SDM77	Male	8.3	9.6	M1/LPMCd	BDA/2	0.8	2.07	23.70	33

TABLE 2.

Contralateral Bouton Counts in Each LPMCd Case by Spinal Lamina[1]

Case	Tracer	Total	V		VI		RMB	VII	VIII	IX	Xc
			Med	Lat	Med	Lat					
SDM57	FD	35,469	0	0	1,269	1,122	583	22,382	8,017	1,218	878
			(0)	(0)	(4)	(3)	(2)	(63)	(23)	(3)	(2)
SDM61	FD	18,892	0	0	927	1,941	1,179	11,982	841	1,602	420
			(0)	(0)	(5)	(10)	(6)	(63)	(4)	(9)	(2)
SDM54	BDA	3,776	0	0	0	331	0	2,384	66	796	199
			(0)	(0)	(0)	(9)	(0)	(63)	(2)	(21)	(5)
SDM72	BDA	812	0	0	0	0	0	812	0	0	0
			(0)	(0)	(0)	(0)	(0)	(100)	(0)	(0)	(0)
SDM72	LYD	464	0	0	0	0	0	464	0	0	0
			(0)	(0)	(0)	(0)	(0)	(100)	(0)	(0)	(0)

[1]Percentages of total are reported in parentheses. Values are rounded to the nearest whole number, except when the value is 0.7 or less. Lat, lateral; Med, medial; RMB, reticulated marginal border.

TABLE 3.

Ipsilateral Bouton Counts in Each LPMCd Case by Spinal Lamina[1]

Case	Tracer	Total	V		VI		RMB	VII	VIII	IX	Xi
			Med	Lat	Med	Lat					
SDM57	FD	9,229	0	0	0	0		4,051	4,545	0	633
			(0)	(0)	(0)	(0)		(44)	(49)	(0)	(7)
SDM61	FD	7,085	0	0	0	0		4,386	2,277	0	422
			(0)	(0)	(0)	(0)		(62)	(32)	(0)	(6)
SDM54	BDA	1,389	0	0	0	0		926	463	0	0
			(0)	(0)	(0)	(0)		(67)	(33)	(0)	(0)
SDM72	BDA	232	0	0	0	0		58	174	0	0
			(0)	(0)	(0)	(0)		(25)	(75)	(0	(0)
SDM72	LYD	0	0	0	0	0		0	0	0	0
			(0)	(0)	(0)	(0)		(0)	(0)	(0)	(0)

[1]Percentages of total are reported in parentheses. Values are rounded to the nearest whole number, except when the value is 0.7 or less. Lat, lateral; Med, medial; RMB, reticulated marginal border.

TABLE 4.

Contralateral Bouton Counts for Case SDM77 (M1- LPMCd transition cortex) and Case SDM72 (LPMCv) by Spinal Lamina[1]

Case	Tracer	Total	V		VI		RMB	VII	VIII	IX	Xc
			Med	Lat	Med	Lat					
SDM77	BDA	7,765	0	0	157	105	209	5,776	577	785	156
			(0)	(0)	(2)	(1)	(3)	(74)	(7)	(10)	(2)
SDM72	FD	6,162	0	231	0	924	1,310	2,618	925	0	154
			(0)	(4)	(0)	(15)	(21)	(42)	(15)	(0)	(2)

[1]Percentages of total are reported in parentheses. Values are rounded to the nearest whole number, except when the value is 0.7 or less. Lat, lateral; Med, medial; RMB, reticulated marginal border.

TABLE 5.

Ipsilateral Bouton Counts for Case SDM77 (M1- LPMCd transition cortex) and Case SDM72 (LPMCv) by Spinal Lamina[1]

Case	Tracer	Total	V		VI		RMB	VII	VIII	IX	Xi
			Med	Lat	Med	Lat					
SDM 77	BDA	1,153	0	0	0	0	0	157	787	0	209
			(0)	(0)	(0)	(0)	(0)	(14)	(68)	(0)	(18)
SDM 72	FD	2,697	0	0	0	0	0	1,387	1,233	0	77
			(0)	(0)	(0)	(0)	(0)	(51)	(46)	(0)	(3)

[1]Percentages of total are reported in parentheses. Values are rounded to the nearest whole number, except when the value is 0.7 or less. Lat, lateral; Med, medial; RMB, reticulated marginal border.